Coherent Control of Ultracold Photoassociation
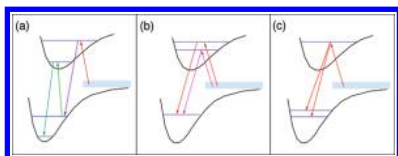
Christiane P. Koch*,† and Moshe Shapiro*,‡

†Theoretische Physik, Universität Kassel, Heinrich-Plett-Strasse 40, 34132 Kassel, Germany
‡Department of Chemistry, University of British Columbia, Vancouver, Canada V6T 1Z1, and Department of Chemical Physics, The Weizmann Institute, Rehovot, Israel 76100

CONTENTS

1. INTRODUCTION

Photoassociation, forming molecules from ultracold atoms using laser light, is a prime example of coherent control: The process is complex and poses many challenges, yet typically the molecular structure is simple enough to identify pathways for control. Laser cooling schemes that work for atoms[1–5] tend to fail for molecules, mainly due to the presence of many near-resonance lines and the fact that other degrees of freedom, in addition to translation (rotations, vibrations, etc.), must be cooled. Though there are a number of viable suggestions[6–9] and first experimental demonstrations[10,11] to radiatively cool the internal degrees of freedom of molecules using light, such methods do not address the issue of cooling the *translational* degrees of freedom. Translational cooling schemes rely on a closed cycling transition which may be found if a rich internal level structure is accidentally absent[12] or can be avoided.[13]

Rather than cool warm molecules, one can try to *synthesize* cold molecules by associating cold atoms using light or a magnetic field. The molecules thus formed are expected to maintain the translational temperature of the recombining atoms, because the center-of-mass motion remains unchanged in the association process (save for the little momentum imparted by a single photon). In the context of forming ultracold molecules, photoassociation was first proposed by Julienne et al.,[14–16] who envisioned a multistep process. The first step involves the free-to-bound excitation of scattering states of an ultracold trapped atom pair to a weakly bound vibrational level in an electronically excited molecular state. This is followed by a bound–bound spontaneous emission to the ground electronic state. Depending on the properties of the potential energy curve of the electronically excited state, the spontaneous emission leads to transitions into weakly bound vibrational levels of the electronic ground state[17–21] or redissociation into atoms which leave the trap.

An undesirable feature of this scheme is that the spontaneous nature of the second step allows the molecules to end up in an incoherent mixture of a large range of vibrational levels. As a consequence, the use of *stimulated* emission, either in an adiabatic passage[22–34] or a nonadiabatic scheme[35–41] as discussed below, was suggested as a way of channeling populations to the particular final molecular state of interest.

The process can be efficiently executed as an adiabatic passage from a continuum (APC) to the final molecular bound state of interest. As in bound–bound AP, central to the APC is the formation of a photoassociation "dark state". This "light-dressed" state, once formed, is impervious to further actions of the light fields. When the light fields are applied as pulses, APC results due to the dark state changing its nature by "following" the makeup of the applied pulses from that of a scattering state of the associating atoms to that of a molecular bound state. Following the theory discussed below, such dark states have been observed experimentally.[42–45] Moreover, adiabatic passage has been successfully employed to transfer so-called

"Feshbach molecules",[46,47] first into deeply bound levels[48,49] and then into their rovibronic ground state.[45,50−52] The starting point for the stimulated Raman adiabatic passage (STIRAP) were extremely weakly bound molecules obtained by ramping a magnetic field over a Feshbach resonance. Magnetoassociation followed by STIRAP has been shown to be a very promising way of creating a high density of ultracold molecules in their ground internal state.

As an alternative to adiabatic passage, repeated sequences of short laser pulses may be employed to form ground state molecules in a nonadiabatic way. The scenario is based on a pump−dump process where a first pulse photoassociates molecules, forming a time-dependent wave packet in an electronically excited state. The wave packet travels toward shorter interatomic separation where a time-delayed dump pulse can catch it, transferring the molecules to the electronic ground state. The pulses may be shaped to reach a specific target level. This coherent pump−dump process needs to be combined with a dissipative step in order to accumulate the photoassociated molecules over many cycles.

Photoassociation of ultracold molecules represents a simple example of a binary reaction under specific, very favorable conditions: At ultracold temperatures the quantum nature of the atoms is becoming visible. At the very lowest temperatures realized to date, where the quantum purity of the ensemble of atoms is highest, adiabatic passage is the most promising approach, in particular in conjunction with a Feshbach resonance. At temperatures in the μK regime, well above quantum degeneracy, it is not possible to address the whole ensemble of scattering atoms all at once. The pump−dump approach to photoassociation, repeated many times and combined with a dissipative process ensuring accumulation of the molecules, is best suited to these conditions. The higher translational temperatures are balanced by a larger number of atoms that can be photoassociated.

The structure of this review is as follows: We first discuss adiabatic passage photoassociation in section 2. Starting from population transfer *to* the continuum in section 2.1 and introducing the adiabatic approximation for the continuum in section 2.2, the concept of adiabatic passage to the continuum is applied to photo*association* in section 2.3. It is combined with STIRAP in section 2.4 and extended to include several interfering pathways in section 2.5. Section 3 gives an overview of experimental realizations of molecule formation using adiabatic passage. A review of short-pulse photoassociation using a repeated pump−dump sequence is presented in section 4, with section 4.1 discussing the choice of the pulse parameters. Sections 4.2 and 4.3 present two control schemes to enhance the overall photoassociation efficiency—controlling a scattering resonance in order to enhance the photo-association/pump step and Franck−Condon engineering in order to improve the stabilization/dump step. Femtosecond photoassociation experiments and their theoretical modeling are described in section 4.4, with further prospects opened by these experiments for the study of many-body pair correlations in dilute gases discussed in section 4.5. Concluding remarks are made in section 5.

2. ADIABATIC PASSAGE PHOTOASSOCIATION

2.1. Population Transfer to the Continuum by Two-Photon Processes

To introduce the theoretical framework of this review, we first examine the case of resonantly enhanced two-photon *dissociation*. We consider a molecule, initially ($t = 0$) in state $|E_1\rangle$ of the material Hamiltonian H_M, excited to $|E,\mathbf{n}^-\rangle$, a continuum of eigenstates of H_M. Here E is the (final material) energy, with $\mathbf{n}$ denoting the other quantum numbers which characterize the *completely dissociated* system. The − superscript is a reminder that complete dissociation occurs only asymptotically, as $t \to \infty$. The dissociation is perceived to occur due to the combined action of *two* laser pulses $\mathbf{E}_1$ and $\mathbf{E}_2$ of central frequencies ω_1 and ω_2. We assume that ω_1 is in near resonance with the transition from $|E_1\rangle$ to $|E_2\rangle$, an intermediate bound state of H_M, and that ω_2 is in near resonance with the transition from $|E_2\rangle$ to the continuum.

The total matter + radiation Hamiltonian is given in the dipole approximation as

$$H_{\text{total}} = H_M - \mathbf{d}_1\varepsilon_1\mathcal{E}_1 - \mathbf{d}_2\varepsilon_2\mathcal{E}_2 \tag{1}$$

where $\mathbf{d}_i\varepsilon_i$ is the projection of dipole moment $\mathbf{d}_i$ on polarization direction ε_i, with $i = 1, 2$. We now solve the time-dependent Schrödinger equation,

$$i\hbar\,\partial\Psi/\partial t = H_{\text{total}}\Psi \tag{2}$$

by expanding Ψ, the total wave function, as

$$|\Psi(t)\rangle = b_1(t)|E_1\rangle \exp(-iE_1 t/\hbar) + b_2(t)|E_2\rangle$$
$$\exp(-iE_2 t/\hbar) + \sum_\mathbf{n} \int dE\, b_{E,\mathbf{n}}(t)|E, \mathbf{n}^-\rangle$$
$$\exp(-iEt/\hbar) \tag{3}$$

We obtain a set of first-order differential equations for the expansion coefficients,

$$db_1/dt = i\Omega_1^*(t) \exp(-i\Delta_1 t)b_2(t) \tag{a}$$

$$db_2/dt = i\Omega_1(t) \exp(i\Delta_1 t)b_1(t) + i\int dE \tag{b}$$
$$\sum_\mathbf{n} \Omega_{2,E,\mathbf{n}}(t) \exp(-i\Delta_E t)b_{E,\mathbf{n}}(t)$$

$$db_{E,\mathbf{n}}/dt = i\Omega_{2,E,\mathbf{n}}^*(t) \exp(i\Delta_E t)b_2(t), \tag{c}$$
$$\text{for all } E \text{ and } \mathbf{n} \tag{4}$$

where

$$\Omega_1(t) \equiv \langle E_2|d_1\hat{\varepsilon}_1|E_1\rangle S_1(t)/\hbar,$$
$$\Omega_{2,E,\mathbf{n}}(t) \equiv \langle E_2|d_2\hat{\varepsilon}_2|E, \mathbf{n}^-\rangle \mathcal{E}_2(t)/\hbar,$$
$$\Delta_1 \equiv (E_2 - E_1)/\hbar - \omega_1, \quad \Delta_E \equiv (E - E_2)/\hbar - \omega_2 \tag{5}$$

and $S_i(t)$ are the pulse envelopes defined as

$$\mathcal{E}_i(t) \equiv \text{Re} S(t)_i \exp(-i\omega_i t) \tag{6}$$

We can eliminate the continuum equations by substituting the formal solution of eq 4c,

$$b_{E,\mathbf{n}}(t) = i\int_0^t dt'\, \Omega_{2,E,\mathbf{n}}^*(t') \exp(i\Delta_E t')b_2(t') \tag{7}$$

into eq 4b to obtain

$$\frac{d}{dt}b_2 = i\Omega_1(t)\exp(i\Delta_1 t)b_1(t)$$
$$- \sum_{\mathbf{n}}\int dE\, \Omega_{2,E,\mathbf{n}}(t)\exp(-i\Delta_E t)\int_0^t dt'$$
$$\Omega_{2,E,\mathbf{n}}^*(t')\exp(i\Delta_E t')b_2(t') \tag{8}$$

Assuming that the continuum is "slowly varying" or "flat" in what might be called the "slowly varying continuum approximation" (SVCA),

$$\langle E_2|d_2\cdot\hat{\varepsilon}_2|E,\mathbf{n}^-\rangle \approx \langle E_2|d_2\cdot\hat{\varepsilon}_2|E_L,\mathbf{n}^-\rangle \tag{9}$$

where E_L is some constant energy, we obtain that

$$\int dE\sum_{\mathbf{n}}|\langle E_2|d_2\hat{\varepsilon}_2|E,\mathbf{n}^-\rangle|^2\exp(-i\Delta_E(t-t'))$$
$$\approx \sum_{\mathbf{n}}|\langle E_2|d_2\hat{\varepsilon}_2|E_L,\mathbf{n}^-\rangle|^2\int dE\exp(-i\Delta_E(t-t'))$$
$$= \sum_{\mathbf{n}}|\langle E_2|d_2\hat{\varepsilon}_2|E_L,\mathbf{n}^-\rangle|^2 2\pi\delta(t-t') \tag{10}$$

Substituting eq 9 into eq 8 and remembering that $\int_0^t dt'\,\delta(t-t') = 1/2$, we obtain that

$$\frac{db_2}{dt} = i\Omega_1(t)\exp(i\Delta_1 t)b_1(t) - \Omega_2^I(t)\,b_2(t) \tag{11}$$

where

$$\Omega_2^I(t) = \pi\sum_{\mathbf{n}}|\langle E_L,\mathbf{n}^-|d_2\hat{\varepsilon}_2|E_2\rangle\mathcal{E}_2(t)|^2/\hbar \tag{12}$$

Coupled with eq 4c, we obtain a simple set of ordinary differential equations for $b_1(t)$ and $b_2(t)$.

2.2. The Adiabatic Approximation for a Final Continuum Manifold

Equations 4a and 11 can be written in matrix notation by defining

$$\underline{b} \equiv (\exp(i\Delta_1 t)b_1, b_2)^{\mathrm{T}} \tag{13}$$

and

$$\mathbf{H} = \begin{pmatrix} \Delta_1 & \Omega_1^* \\ \Omega_1 & i\Omega_2^I \end{pmatrix} \tag{14}$$

as

$$\frac{d\underline{b}}{dt} = i\mathbf{H}\cdot\underline{b} \tag{15}$$

Assuming that Ω_1 is real, we obtain the adiabatic solutions to eq 15 by diagonalizing the $\mathbf{H}$ matrix. The presence of the continuum, coupled within the SVCA, results in a complex-symmetric $\mathbf{H}$ matrix. Such matrices are diagonalizable using complex-orthogonal matrices $\mathbf{U}$, satisfying

$$\mathbf{U}(t)\cdot\mathbf{U}^{\mathrm{T}}(t) = \mathbf{I} \tag{16}$$

Note that $\mathbf{U}$ must be nonunitary on physical grounds in order to allow flux loss to the continuum. The 2×2 complex orthogonal $\mathbf{U}$ matrix obtained here can be parametrized in terms of a single complex "mixing angle" α, where

$$\mathbf{U} = \begin{pmatrix} \cos\alpha & \sin\alpha \\ -\sin\alpha & \cos\alpha \end{pmatrix} \tag{17}$$

and

$$\alpha(t) = \frac{1}{2}\arctan\left(\frac{2\Omega_1}{i\Omega_2^I - \Delta_1}\right) \tag{18}$$

Operating with $\mathbf{U}^{\mathrm{T}}(t)$ on eq 15, and defining

$$\underline{a}(t) = \mathbf{U}^{\mathrm{T}}(t)\cdot(t) \tag{19}$$

we obtain that

$$\frac{d}{dt}\underline{a} = \{i\lambda(t) + \mathbf{A}\}\cdot\underline{a} \tag{20}$$

with

$$\mathbf{A} \equiv \frac{d\mathbf{U}^{\mathrm{T}}(t)}{dt}\cdot\mathbf{U} = \begin{pmatrix} 0 & -\dot{\alpha} \\ \dot{\alpha} & 0 \end{pmatrix} \tag{21}$$

The adiabatic solutions are given by

$$\underline{a}(t) = \exp\left\{i\int_0^t \lambda(t')\,dt'\right\}\underline{a}(0) \tag{22}$$

with the elements of the diagonal eigenvalue matrix, λ, given by

$$\lambda_{1,2} = \frac{1}{2}\{\Delta_1 + i\Omega_2^I \pm [(\Delta_1 - i\Omega_2^I)^2 + 4|\Omega_1|^2]\} \tag{23}$$

Using eqs 13 and 19, and imposing the initial condition, $\underline{b}(0) = (1, 0)$, we obtain for the $b_1(t)$ and $b_2(t)$ coefficients

$$b_1(t) = \{U_{1,1}(t)\exp[i\int_0^t \lambda_1(t')\,dt']U_{1,1}(0)$$
$$+ U_{2,1}(t)\exp[i\int_0^t \lambda_2(t')\,dt']U_{2,1}(0)\}\exp(-i\Delta_1 t)$$

$$b_2(t) = U_{1,2}(t)\exp[i\int_0^t \lambda_1(t')\,dt']U_{1,1}(0)$$
$$+ U_{2,2}(t)\exp[i\int_0^t \lambda_2(t')\,dt']U_{2,1}(0) \tag{24}$$

If both lasers are assumed to be off initially, i.e. $S_1(0) = S_2(0) = 0$, we have that $\alpha(0) = 0$. Hence $U_{1,1}(0) = 1$, $U_{2,1}(0) = 0$, and

$$\begin{pmatrix} b_1(t) \\ b_2(t) \end{pmatrix} = \begin{pmatrix} \exp(-i\Delta_1 t)\cos\alpha(t) \\ \sin\alpha(t) \end{pmatrix}\exp\left\{i\int_0^t \lambda_1(t')\,dt'\right\} \tag{25}$$

Once $b_2(t)$ is known, the continuum coefficients $b_{E,\mathbf{n}}(t)$ are obtained directly via eq 7.

2.3. Theory of Photoassociation of a Coherent Wave Packet

We now apply the methodology developed for the two-photon dissociation problem to resonantly enhanced *photoassociation*. In photoassociation the initial state is the scattering state and the goal is to transfer the population to the final *bound* state $|E_1\rangle$. We therefore consider a pair of colliding atoms described by scattering states $|E,\mathbf{n}^+\rangle$, with $\mathbf{n}$ incorporating the quantum indices specifying the electronic states of the separated atoms and E being the total collision energy. The $+$ superscript signifies, in contrast with the $-$ states that were previously used to describe dissociation processes, that the *initial* state of the fragments is known.

Following ref 22, we focus attention on a Λ-type system, shown in Figure 1c, subjected to the combined action of two laser pulses of central frequencies ω_1 and ω_2. Here ω_2 is in near-resonance with the transition from the $|E,\mathbf{n}^+\rangle$ continuum
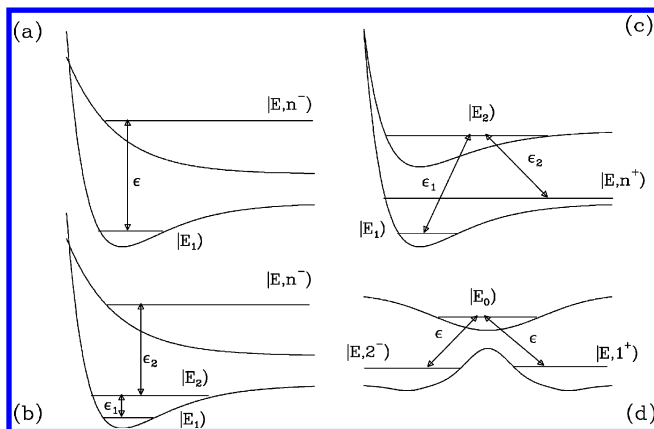
Figure 1. Energy levels and pulses pertaining to (a) one-photon dissociation, (b) resonantly enhanced two-photon dissociation, (c) resonantly enhanced two-photon association, or (d) laser catalysis.

to an intermediate bound state $|E_2\rangle$, and ω_1 is in near-resonance with the transition from $|E_2\rangle$ to $|E_1\rangle$.

With the total Hamiltonian of the system given by eq 1 and the material wave function of the system expanded as in eq 3, we obtain a set of first-order differential equations for the expansion coefficients that is essentially identical to that of eq 4, except that the bound-continuum dipole matrix elements are now of the form $\langle E_2|\mathbf{d}_2 \cdot \varepsilon_2|E,\mathbf{n}^+\rangle$, involving the $|E,\mathbf{n}^+\rangle$, rather than the $|E,\mathbf{n}^-\rangle$, states.

In the photoassociation case, contrary to the dissociation cases discussed above, the continuum is initially populated, i.e., $b_{E,\mathbf{n}}(0) \neq 0$. Hence, the formal solution of eq 4c is now of the following form:

$$b_{E,\mathbf{n}}(t) = b_{E,\mathbf{n}}(t = 0)$$
$$+ i \int_0^t dt' \, \Omega_{2,E,\mathbf{n}}^*(t') \exp(i\Delta_E t') \, b_2(t') \quad (26)$$

Substituting this solution into eq 4b gives

$$db_2/dt = i\Omega_1(t) \exp(i\Delta_1 t) b_1(t) - \Gamma b_2$$
$$+ i \sum_{\mathbf{n}} \int dE \, \Omega_{2,E,\mathbf{n}}(t) \exp(-i\Delta_E t) \, b_{E,\mathbf{n}}(t = 0)$$
$$- \sum_{\mathbf{n}} \int dE \int_0^t dt' \, \Omega_{2,E,\mathbf{n}}(t) \, \Omega^*_{2,E,\mathbf{n}}(t')$$
$$\exp[-i\Delta_E(t - t')]b_2(t') \quad (27)$$

where Γ is the spontaneous emission rate.

If the molecular continuum is unstructured, we can invoke the SVCA and replace the energy-dependent bound-continuum dipole matrix-elements by their value at the pulse center, given (in the Λ configuration of Figure 1c) as $E_L = E_2 - \hbar\omega_2$. This is the case, for example, for Na_2 at threshold energies, where the bound-continuum dipole matrix-elements vary with energy by less than 1% over a typical nanosecond-pulse bandwidth. Within the SVCA, eq 26 becomes

$$\frac{db_2}{dt} = i\Omega_1(t) \exp(i\Delta_1 t) b_1(t) - [\Gamma + \Omega_2^I(t)]b_2(t) + iF(t) \quad (28)$$

where

$$F(t) \equiv \mathcal{E}_2(t) \, \bar{d}_2(t)/\hbar \quad (29)$$

with

$$\bar{d}_2(t) \equiv \sum_{\mathbf{n}} \int dE\langle E_2|\mathbf{d}_2 \cdot \varepsilon_2|E, \mathbf{n}^+\rangle \times \exp(-i\Delta_E t)$$
$$b_{E,\mathbf{n}}(t = 0) \quad (30)$$

and where $\Omega_2^I(t)$ is defined as in eq 12. Equations 28 and 8 can be expressed in matrix notation as

$$\frac{d}{dt}\underline{b} = i\{\mathbf{H}' \cdot \underline{b}(t) + \underline{f}\} \quad (31)$$

where

$$\underline{f}(t) = (0, F(t))^{\mathbf{T}} \quad (32)$$

with $\underline{b}$ as defined in eq 13 and

$$\mathbf{H}' = \mathbf{H} + \begin{pmatrix} 0 & 0 \\ 0 & i\Gamma \end{pmatrix}$$

with $\mathbf{H}$ defined in eq 1.

The "*net association rate*" $R(t)$ is the rate of population-change in the bound manifold, given by $d/dt(|b_1|^2 + |b_2|^2)$. It can be written, using eq 31 and its complex conjugate, as

$$R(t) = \frac{d}{dt}(|b_1|^2 + |b_2|^2)$$
$$= \frac{d}{dt}|\underline{b}|^2$$
$$= \underline{b}^\dagger \cdot \left(\frac{d}{dt}\underline{b}\right) + \left(\frac{d}{dt}\underline{b}^\dagger\right) \cdot \underline{b}$$
$$= i\{\underline{b}^\dagger \cdot (\mathbf{H} - \mathbf{H}^\dagger) \cdot \underline{b} + \underline{b}^\dagger \cdot \underline{f} - \underline{f}^\dagger \cdot \underline{b}\}$$
$$= 2I_m[F^*(t)b_2(t)] - 2\Omega_2^I(t)|b_2(t)|^2 \quad (33)$$

The first term in eq 33 represents the association rate,

$$R_{\text{rec}}(t) \equiv 2I_m[F^*(t) \, b_2(t)] \quad (34)$$

and the second term is the back-dissociation rate,

$$R_{\text{diss}}(t) \equiv 2\Omega_2^I(t)|b_2(t)|^2 \quad (35)$$

As expected, the net association rate (eq 33) is the difference between the association rate and the back-dissociation rates.

We can solve eq 31 adiabatically by diagonalizing the $\mathbf{H}'$ matrix. Operating with $\mathbf{U}(t)$ on eq 31, with $\underline{a}(t)$ defined as in eq 19, we obtain that

$$\frac{d}{dt}\underline{a} = \{i\lambda(t) + \mathbf{A}\} \cdot \underline{a} + i\underline{g} \quad (36)$$

where the source-vector $\underline{g}$ is given as

$$\underline{g}(t) = \begin{pmatrix} F(t) \, U_{1,2}(t) \\ F(t) \, U_{2,2}(t) \end{pmatrix} = \begin{pmatrix} F(t) \sin\theta(t) \\ F(t) \cos\theta(t) \end{pmatrix} \quad (37)$$

Invoking the adiabatic approximation, we obtain from eq 36 that

$$\frac{d}{dt}\underline{a} = i\lambda(t) \cdot \underline{a}(t) + i\underline{g}(t) \quad (38)$$

In the association process the initial conditions are such that

$$\underline{a}(t = 0) = 0 \quad (39)$$

so that the adiabatic solutions are

$$\underline{a}(t) = \mathbf{v}(t) \cdot \underline{q}(t) \tag{40}$$

where

$$\mathbf{v}(t) = \exp\left\{i \int_0^t \lambda(t') \, dt'\right\} \tag{41}$$

and

$$\underline{q}(t) = i \int_0^t \mathbf{v}^{-1}(t') \cdot \underline{g}(t') \, dt' \tag{42}$$

with $\lambda_{1,2}$ given by eq 23.

Using eqs 19 and 13, we obtain for the $b_1(t)$ and $b_2(t)$ coefficients in the adiabatic approximation:

$$b_1(t) = i\Big\{\cos\theta(t) \int_0^t \exp\Big[i \int_{t'}^t \lambda_1(t'') \, dt''\Big] F(t')$$
$$\sin\theta(t') \, dt' - \sin\theta(t) \int_0^t \exp\Big[i \int_{t'}^t \lambda_2(t'') \, dt''\Big]$$
$$F(t') \cos\theta(t') dt'\Big\} \exp(-i\Delta_1 t)$$

$$b_2(t) = i\Big\{\sin\theta(t) \int_0^t \exp\Big[i \int_{t'}^t \lambda_1(t'') \, dt''\Big] F(t')$$
$$\sin\theta(t') \, dt' + \cos\theta(t) \int_0^t \exp\Big[i \int_{t'}^t \lambda_2(t'') \, dt''\Big]$$
$$F(t') \cos\theta(t') \, dt'\Big\} \tag{43}$$

Given $b_2(t)$, the (channel-specific) continuum coefficients $b_{E,\mathbf{n}}(t)$ are obtained directly via eq 26.

It is instructive to study the adiabatic solution when there is insignificant temporal overlap between the two laser pulses. Assuming in that case that the ω_2 pulse precedes the ω_1 pulse, we have during the ω_2 pulse that $S_2 \gg S_1$; hence, by eq 23, $\lambda_1 \approx \Delta_1$, $\lambda_2 \approx i[\Gamma + \Omega_2^I]$, and $\theta(t) = 0$. Substituting these values into eq 43 gives that during the ω_2 pulse (when the ω_1 pulse is off):

$$b_1(t) = 0;$$

$$b_2(t) = i \int_0^t \exp\Big\{-\int_{t'}^t [\Gamma + \Omega_2^I(t'')] \, dt''\Big\} F(t') \, dt' \tag{44}$$

From eq 29 it is clear that the source term $F(t)$ is linearly proportional to the pulse amplitude. On the other hand, since $\Omega_2 > 0$ and $t' < t$, the $\exp\{-\int_{t'}^t \Omega_2^I(t'') \, dt''\}$ factor (describing dissociation back to the continuum) decays exponentially with increasing intensity. Thus, merely increasing the laser power does not necessarily increase the association yield. There exists some optimal intensity, beyond which the association probability decreases. Below we display some pulse configurations for a realistic case of photoassociation.

As an example of this formulation, we consider pulsed photoassociation of a coherent wave packet of cold Na atoms.[22] The colliding atoms are described by an (energetically narrow) normalized Gaussian packet of $J = 0$ radial waves:

$$|\Psi(t = 0)\rangle = \int dE \, b_E(t = 0)|E, 3s + 3s\rangle \tag{45}$$

where $|E, 3s + 3s\rangle$ are the scattering Na–Na s-waves with the atoms in the 3s state, and b_E at time zero is taken as

$$b_E(t = 0) = (\delta_E^2 \pi)^{-1/4} \exp\{-(E - E_{col})^2 / 2\delta_E^2 + i\Delta_E t_0\} \tag{46}$$

Here, t_0 denotes the instant of maximum overlap of the Na + Na wave packet with the $|E_2\rangle$ state. In the simulations, E_{col}, the mean collision energy, varies between $E_{col} = 0.00695$ cm^{-1} –

0.0695 cm$^{-1} \approx 0.01K - 0.1K$ and the wave packet widths, δ_E, vary over the range $\delta_E = 10^{-4}$ cm^{-1} to 10^{-3} cm^{-1}. State $|E_1\rangle$ is chosen as the $(X^1\Sigma_g^+, \nu = 0, J = 0)$ state and $|E_2\rangle$ as the $(A^1\Sigma_u^+, \nu' = 34, J = 1)$ state, as shown in Figure 2. Thus, the combined
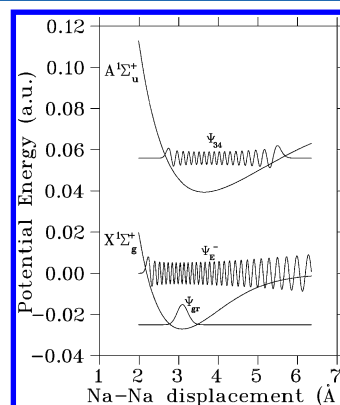

Figure 2. Potentials and vibrational wave functions used in the simulation of the Na + Na two-photon association. Reprinted from Figure 2 of ref 22. Copyright 1997 American Institute of Physics.

effect of the two laser pulses is the transfer of population from the continuum to the ground vib-rotational state $(X^1\Sigma_g^+, \nu = 0, J = 0)$, with the bound $(A^1\Sigma_u^+, \nu' = 34, J = 1)$ state acting as an intermediate state. In order to minimize spontaneous emission losses, we concentrate on the "counterintuitive"[53] scheme where the "dump" pulse $S_1(t)$ is applied *before* the $S_2(t)$ "pump" pulse.

As discussed in section 2.1, when either the final or initial state is in the continuum, the Rabi frequency is imaginary, which changes the range of validity of the adiabatic approximation. For example, it does not necessarily hold even for "large area" $\int \Omega \, dt$ pulses.[54,55] For example, as shown in Figure 2, in the presence of a continuum, the adiabatic approximation tends to break down for small detunings. Despite this fact, we show below that, with the proper choice of pulse parameters, it is possible to transfer the entire population contained in the continuum wave packet to the ground state, while keeping the intermediate state population low at all times. Moreover, for such pulse parameters, the adiabatic solutions (eq 43) are in perfect agreement with exact-numerical solutions.[22]

A typical population evolution is shown in Figure 3, which is obtained with pulse intensities of order 10^8 W/cm^2 and pulse durations of several nanoseconds. Clearly demonstrated is the completeness of the continuum-to-bound population transfer, which proceeds with essentially no population in the intermediate state. These findings are very similar to the situation in the three-bound-states STIRAP process. In other words, at sufficiently high intensities, a *dark state* that is completely analogous to that of bound state STIRAP is formed in the photoassociation case as well. Experimental evidence for the formation of such dark states has been presented[44,45] and will be discussed in greater detail below.

The pulse intensities used are sufficiently small to avoid unwanted photoionization, photodissociation, and other strong field parasitic processes. However, working with pulses requires that the atoms be sufficiently close to one another during the laser pulse that they can be recombined. In other words, the initial wave packet of continuum states considered here must be synchronized in time and in duration with the recombining
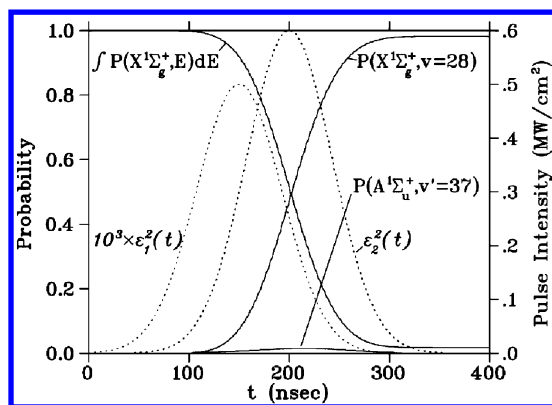
Figure 3. The appearance of a "dark state" in photoassociation via a "counterintuitive" pulse sequence. Shown, as a function of time, are the integrated population of the wave packet of initial continuum states, the population of the $v = 34$, $J = 1$ intermediate state, and the population of the $v = 0$, $J = 0$ final ground-state. Clearly seen is that at the intensities used there is essentially no population in the intermediate state, in complete similarity to the three-bound-states STIRAP process. Dashed lines are the intensity profiles of the two Gaussian pulses, whose central frequencies are $\omega_1 = 18{,}143.775$ cm^{-1} and $\omega_2 = 12{,}277.042$ cm^{-1} (i.e., $\Delta_1 = \Delta_{Ecol} = 0$). The maximum intensity of the dump pulse is 1.6×10^8 W/cm^2, and that of the pump pulse is 3.1×10^9 W/cm^2. Both pulses last 8.5 ns. The pump pulse peaks at $t_0 = 20$ ns, the peak time of the Na + Na wave packet. The dump pulse peaks 5 ns before that time. The initial kinetic energy of the Na atoms is 0.0695 cm^{-1} (or 0.1 K). Reprinted from Figure 4 of ref 22. Copyright 1997 American Institute of Physics.

pulses. It is therefore of interest to see whether it is possible to employ longer pulses (of lower intensity) in order to increase the absolute number of recombining atoms and the overall duty cycle of the process.

Use of pulses of different intensity and different durations is illustrated for the "counterintuitive" scheme in Figure 4, where the rates of association [R_{rec} of eq 34], back-dissociation [R_{diss} of eq 35], and the net association rate [$R(t)$ of eq 33] are plotted as a function of time. A short-pulse case is shown in Figure 4a, and a long-pulse case, with a more spread out wave packet, is shown in Figure 4b. Both figures appear identical, though in Figure 4b the abscissa is scaled up by a factor of 10 and the ordinate is scaled down by a factor of 10.

The scaling behavior demonstrated in Figure 4 is due to the existence of exact scaling relations in eq 31. This scaling is obtained when the initial wave packet-width and the pulse intensities are scaled down as

$$\delta_E \to \frac{\delta_E}{s}, \qquad S_1^0 \to \frac{S_1^0}{s}, \qquad S_2^0 \to \frac{S_2^0}{\sqrt{s}} \qquad (47)$$

and the pulse durations are scaled up as

$$\Delta t_{1,2} \to \Delta t_{1,2} s \qquad (48)$$

It follows from eq 12 that under these transformations

$$F(t) \to \overline{F}_2(t) = \frac{F(t/s)}{s}; \qquad \frac{\Omega_{1,2}(t/s)}{s}$$

and eq 31 becomes

$$\frac{d}{dt/s} \underline{b}' = i\{\mathbf{H}'(t/s) \cdot \underline{b}' + \mathbf{f}(t/s)\} \qquad (49)$$
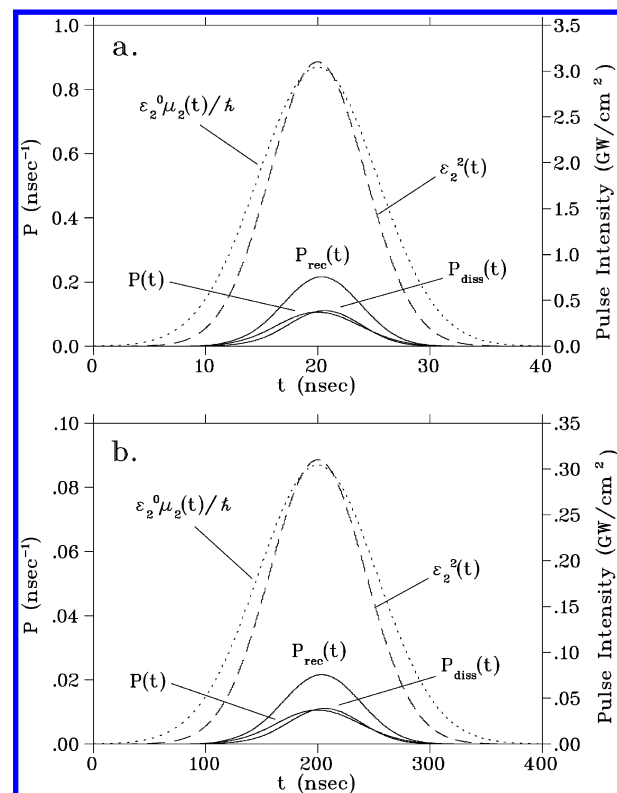

Figure 4. Rates of association (P_{rec}), back-dissociation (P_{diss}), and total molecule-formation (P) vs t in the "counterintuitive" scheme. Dashed lines are the pulse intensity profile; dotted lines denote the effective Rabi frequency $S_2^0 \overline{d}_2(t)/\hbar$, where S_2^0 is the peak pulse intensity. (a) Initial wave packet width of $\delta_E = 10^{-3}$ cm^{-1} and other pulse parameters as in Figure 3. (b) The dynamics scaled by $s = 10$: Initial wave packet width of $\delta_E = 10^{-4}$ cm^{-1}; both pulses lasting 85 ns; the pump pulse peaking at $t_0 = 200$ ns and the dump pulse peaking at 50 ns before that time. The peak intensity of the dump pulse is 1.6×10^6 W/cm^2, and that of the pump pulse is 3.1×10^8 W/cm^2. Reprinted from Figure 5 of ref 22. Copyright 1997 American Institute of Physics.

where $\underline{b}'$ denotes the vector of solutions of the scaled equations. Thus, the scaled coefficients at time t are identical to the unscaled coefficients at time t/s.

One of the results of the above scaling relations is that the pulses' durations can be made longer and their intensities concomitantly scaled down, without changing the final population-transfer yields. As noted above, lengthening of the pulses is beneficial because it causes more atoms to recombine within a given pulse.

There is a range of pulse parameters (such as the pulse area, $\Omega_{2,EL}\Delta t_2$) that maximizes the association yield for a *fixed* initial wave packet. For both the "intuitive" and the "counterintuitive" schemes, there is a clear maximum at a specific pulse area; merely increasing the pulse intensity does not lead to an improved association yield. We can attribute this behavior to the fact that the association rate (R_{rec} of eq 34) increases linearly with increasing pulse intensity, whereas the dissociation rate (R_{diss} of eq 35) increases exponentially with the intensity. Hence, as long as the energetic width of the initial wave packet stays fixed, the association yield turns over with increasing pulse area. The turnover point is different for the two pulse schemes: in the "counterintuitive" case it occurs at a much higher intensity (area).
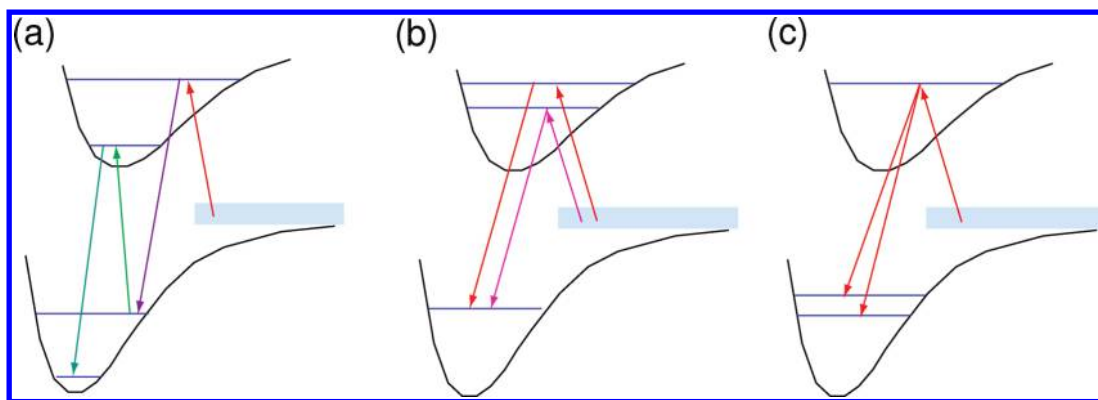
Figure 5. Three combinations of AP pairs discussed in the text.

The existence of a window of intensities for efficient association explains why it is not possible to increase the pulse durations *ad infinitum*, i.e., to work with CW light. As $\Delta t_{1,2}$ increases, it follows from eq 47 that $|S_2/S_1|^2$ must also increase. Since $|S_1|^2$ cannot vanish, $|S_2|^2$ must diverge if one is to stay within the windows of intensities for efficient association in the CW limit. Hence, radiative association as described in this section cannot take place in the CW regime.

There are various experimental demonstrations of photoassociation via two-photon transition as discussed above.[56−60] Evidence that counterintuitive pulse ordering results in large photoassociation cross sections has also been reported,[42−45,52] as discussed in greater detail below.

2.4. Photoassociation by the Consecutive Application of APC and STIRAP

One of the drawbacks of the APC scheme discussed above is that for many cases the Franck−Condon (FC) overlaps between the vibrational state excited from the continuum and the ground vibrational state are rather poor, necessitating (as in the Na_2 example above) the use of rather high powers. To overcome this process, we discuss in this section the execution of APC and bound−bound STIRAP *in tandem*.

As a specific example, we consider the photoassociation of two ^{85}Rb atoms colliding on the Rb_2 $X^1\sum_g^+$-potential.[61] One of the possibilities illustrated in Figure 5a is to do so by first executing APC with a pair of laser pulses to transfer, via $|E_2\rangle$ (an intermediate $A^1\Sigma_u/b^3\Pi_u$ vibrational state), a fraction of the continuum population to $|E_1\rangle$ (an (excited) vibrational state of the Rb_2 $X^1\sum_g^+$-state, which is chosen to have good FC factors with the $|E_2\rangle$ state). Later, a bound−bound STIRAP process is used to transfer the population from the $|E_1\rangle$ state to the ground vibrational state. Figure 6 shows the Born−Oppenheimer potentials for the Rb−Rb system. The $X^1\sum_g^+$ and $1^3\Sigma_u^+$ potentials, as well as the spin−orbit coupling terms, are taken from refs 63 and 64.

Due to the presence of a resonance lying just a notch above the continuum threshold,[65,66] the computed low energy s-wave elastic cross section of two ^{85}Rb atoms on the $X^1\sum_g^+$ and $1^3\Sigma_u^+$ potentials is in excess of 5.7×10^6 au^2.[67,68] As shown in Figure 7a, the scattering resonance enhances the photoassociation probability because it increases the amplitude of the continuum wave function in the inner region, thereby augmenting the $X^1\sum_g^+ - A^1\sum_u^+/b^3\prod_u$ continuum-bound FC factors. The increase in the FC factors also means that we need to use much lower laser intensities in order to guarantee adiabaticity.

The dependence of the continuum-bound s-wave FC factors at collision energies of $E \approx 100\mu K$ on the bound $A^1\Sigma_u^+/b^3\Pi_u$
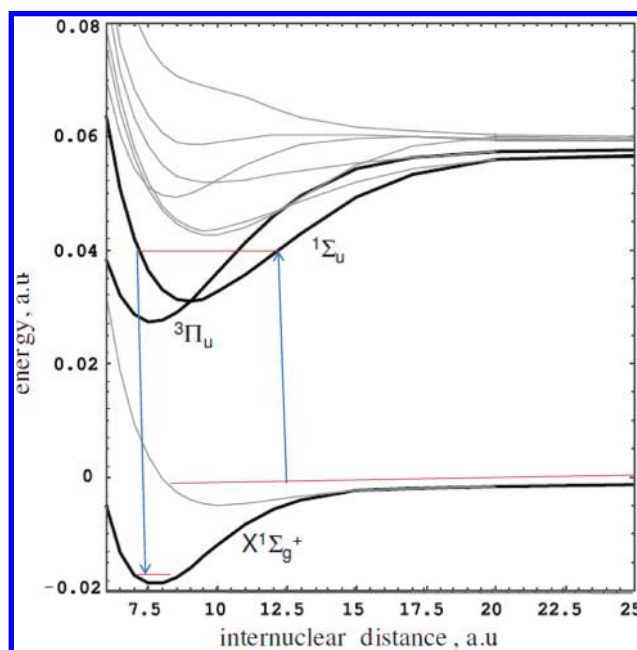

Figure 6. Black lines: Rb_2 Born−Oppenheimer potentials involved in the photoassociation calculations. Gray lines: Other Rb_2 potentials (not used in the calculation). The data shown in the figure are adopted from ref 62.

states energies is shown in Figure 7a. The APC scheme is expected to work best for transitions to bound states lying in the vicinity of the $A^1\Sigma_u^+/b^3\Pi_u(v = 133, J = 1)$ level ($E = 9404$ cm^{-1}), for which the continuum-bound FC factor is as high as 31.5 au. The choice of this level is also based on the availability of large area (and microsecond-long) Nd:YAG lasers at $\lambda = 1064$ nm—in resonance with the continuum-bound transitions to it.

Figure 8 shows an example of photoassociation of a Gaussian wave packet of Rb atoms described by eq 46, whose parameters are: $E_0 = 100\mu K$, $\delta_E = 70\mu K$, and $t_0 = 1150$ ps. The resulting continuum envelope $F_0(t)$ is shown in Figure 8a. In this calculation, the first pair of pulses transfers the entire population of the continuum wave packet to the $X(v = 4, J = 0)$ state (of energy $E = -4001$ cm^{-1}). The pulse durations are chosen so that their spectral widths will roughly coincide with that of the initial continuum wave packet. As shown in Figure 8, the final population of the $X(v = 4, J = 0)$ state is 0.6. If there is no spontaneous emission of the intermediate state (i.e., $\Gamma = 0$),
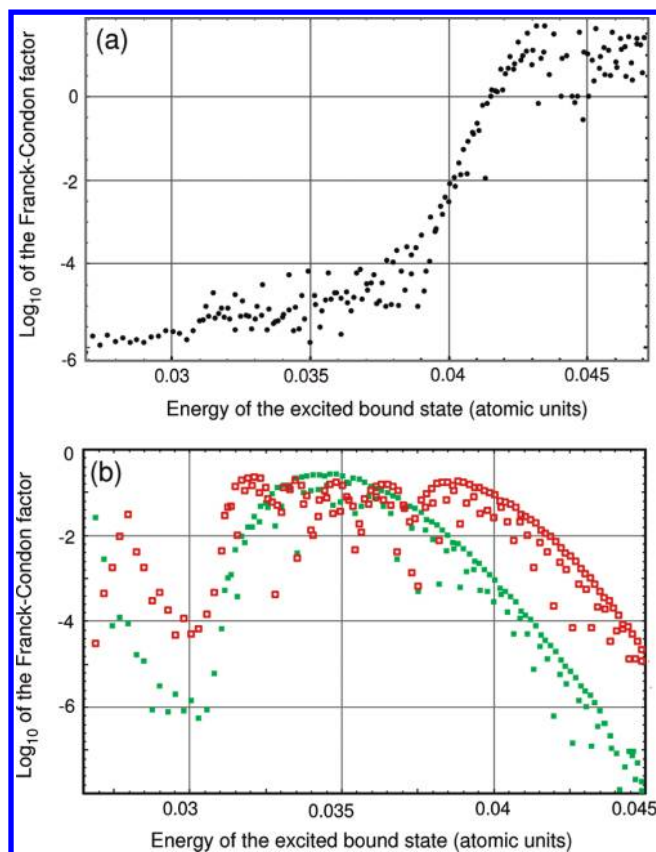
Figure 7. (a) FC factors for the $X^1\sum_g^+ - A^1\sum_u^+/b^3\prod_u$ continuum-bound transitions. (b) FC factors for the $A^1\sum_u^+/b^3\prod_u - X^1\sum_g^+$ bound–bound transitions, for the $v = 0$ (green) and $v = 3$ (red) $X^1\sum_g^+$-vibrational states.
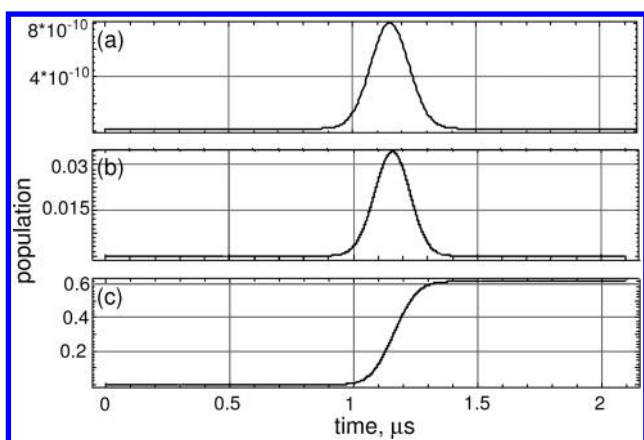

Figure 8. Photoassociation of a coherent wave packet. (a) $|F_0(t)|^2$. (b) The population of the intermediate $A^1\sum_u^+/b^3\prod_u$ state. (c) The population of the $X(v = 4, J = 0)$ target state.

the population of the $X(v = 4, J = 0)$ level reaches values as high as 0.9.

Having populated the $X(v = 4, J = 0)$ state, we now perform a bound–bound STIRAP process (using the pair of pulses of Figure 5a) to execute a complete population transfer to the final, $X(v = 0, J = 0)$, state. In the STIRAP process a pump pulse of center frequency of 11261 cm^{-1} is followed after a delay of 600 ns by a dump pulse of center frequency of 11507 cm^{-1}. These frequencies are in near resonance with an intermediate $A^1\sum_u^+/b^3\prod_u$ vibrational state of energy $E_1 = 7262$ cm^{-1}. As a

result of the process, the population of the $X(v = 4, J = 0)$ state is completely transferred to the $X(v = 0, J = 0)$ state.

To estimate the fraction of atoms photoassociated per pulse, we need to multiply $P(E)$, the photoassociation probability of each colliding pair at energy E, by the number of collisions suffered by a given atom during the pulse. As illustrated in Figure 9, this number is calculated as follows: At a given energy
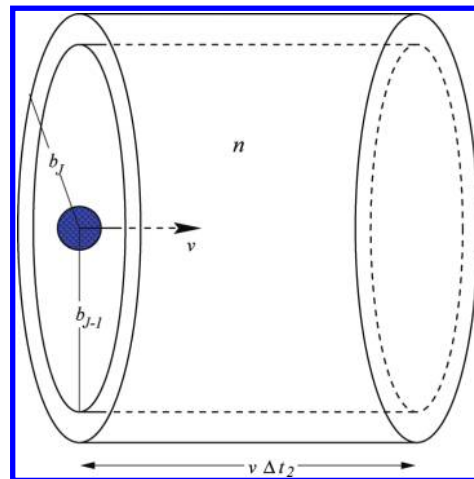

Figure 9. Calculation of the number of atoms in an ensemble of density n of impact parameter b_J that are in close enough vicinity to an atom moving at velocity v to be photoassociated during a pulse lasting Δt_2.

E, the velocity of a given atom is $v = (2E/m)^{12}$ and the distance transversed by it during a pulse of Δt_2 duration is $v\Delta t_2$. The cross section for collision is πb^2, where b is the impact parameter, related to the J partial wave angular momentum as $b = (J + ^1/_2)/p = (J + ^1/_2)/(2mE)^{12}$. Hence, the number of collisions suffered by the atom during the pulse is $N = n\pi b^2 v\Delta t_2$, where n is the density of atoms. Putting all this together, we have for $J = 0$ that the fraction of atoms photoassociated per pulse is

$$f = \frac{P(E)p(2E/m)^{1/2}\Delta t_2}{8mE} = \frac{P(E)\pi\Delta t_2}{4m^{3/2}(2E)^{1/2}} \tag{50}$$

For $\Delta t_2 = 750$ ns, atomic density of $n = 10^{11}$ cm^{-3}, collision energy of $E = 100\ \mu$K, and the ^{85}Rb–^{85}Rb reduced mass of $m = 1823 \times 85/2$ au, we have that $f \approx 2 \times 10^{-7}$ per pulse, in agreement with Figure 10f. Thus, one needs to repeat the pulse sequence about $\sim 5 \times 10^6$ times in order to photoassociate the majority of the ensemble. Since many mode-locked laser sources operate at $\sim 10^6$ pulse per second and above, the above process can be completed in less than 1 min. Here we assume that the photoassociated molecules are removed from the trap for the atoms (and stored in a different trap) before the next pulse sequence arrives.

2.5. Interference between Different Pathways

As in weak field coherent control, the introduction of a number of interfering pathways to the APC process is expected to enhance the population of a desired final state. Below we study two simple interference schemes involving an initial continuum using the "double-Λ"[69] and the "tripod" schemes.

The double-Λ scheme (Figure 5b) consists of performing a two-path photoassociation using two pairs of pulses. Two states, e.g., $|2\rangle \equiv A^1\sum_u^+/b^3\prod_u(v = 133, J = 1)$ and $|3\rangle \equiv A^1\sum_u^+/$
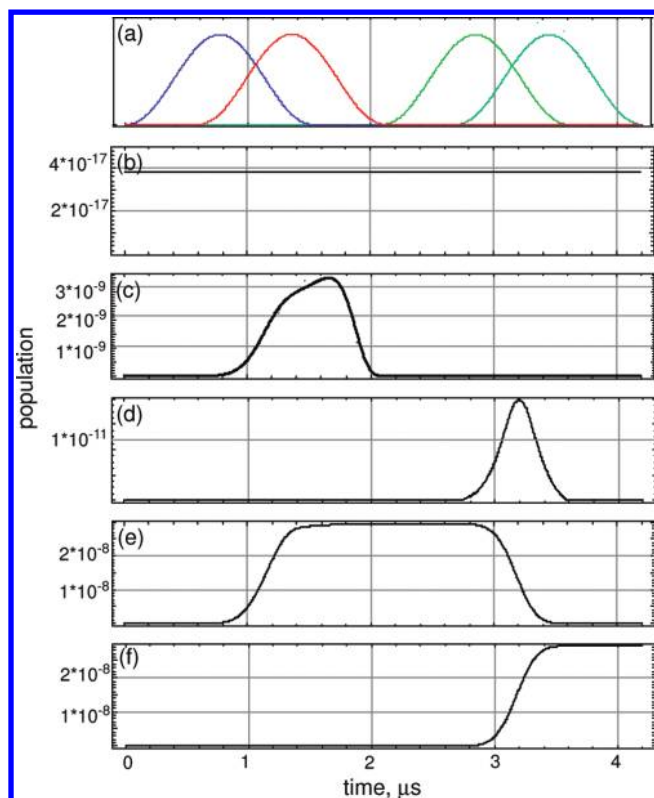
Figure 10. Photoassociation of the atomic ensemble in a trap. (a) Envelopes of the four laser pulses, unscaled. (b) $F_0(t)^2$. (c–f) Bound state populations, weighted over the ensemble, for different bound states. (c) $A^1\Sigma_u/b^3\Pi_u(v = 133, J = 1)$, $E = 9404$ cm^{-1}. (d) $X^1\Sigma_g^+(v = 4, J = 0)$, $E = -4001$ cm^{-1}. (e) $A^1\Sigma_u/b^3\Pi_u(v = 35, J = 1)$, $E = 7262$ cm^{-1}. (f) $X^1\Sigma_g^+(v = 0, J = 0)$, $E = -4236$ cm^{-1}.

$b^3\Pi_u(v = 136, J = 1)$, serve as intermediates leading to, e.g., the final $|1\rangle \equiv X(v = 4, J = 0)$ state. For simplicity, we assume that $\Delta_{12} = \Delta_{13} = \Delta_b$, $\Delta_{E2} = \Delta_{E3} = \Delta_E$, $\Omega_{12} = \Omega_{13} = W_b$, and $\Omega_{E3} = \Omega_{E2} \exp[i\alpha]$. With these assumptions we can write the time-dependent equations analogous to eq 4 as

$$\dot{b}_1 = i\Omega_b^*(b_2 + b_3)e^{-i\Delta_b t}$$

$$\dot{b}_2 = i\Omega_b b_1 e^{i\Delta_b t} - \Gamma(b_2 + e^{-i\alpha}b_3) + i\Omega_E F_0(t)$$

$$\dot{b}_3 = i\Omega_b b_1 e^{i\Delta_b t} - \Gamma(e^{i\alpha}b_2 + b_3) + ie^{i\alpha}\Omega_E F_0(t) \quad (51)$$

Introducing the new amplitude $b_{exc} = b_2 + b_3$, we see that the process is analogous to the single-pathway photoassociation governed by a combined continuum-bound α independent Rabi frequency ranging between 0 and $2\Omega_E$. We find that the decay rate of b_{exc} does depend on α and is lower than the one governing the single-pathway APC. If $\alpha = 0$, then the decay rate for b_{exc} is equal to $2\pi\Omega_E^2$ rather than $\pi(2\Omega_E)^2$.

The role of the relative phase in the double-Λ AP was also checked.[70] Using intensities of $I_{b2} = 3.5 \times 10^3$ W/cm^2 and $I_{E2} = 5 \times 10^3$ W/cm^2 for the two transitions involving the $A^1\Sigma_u^+/b^3\Pi_u(v = 133, J = 1)$ intermediate state, it was found[70] that the maximal yield of AP in the double-Λ passage is higher than that achieved in the single-pathway passage with twice the field strength. The efficiency of double-Λ AP depends on the relative phase between the four Rabi frequencies.

An alternative configuration which takes advantage of interfering pathways is the "tripod" configuration, shown in Figure 5c. On the basis of the bound–bound studies,[71–74] one

expects that the ratio between the Rabi frequencies of the two dump pulses would determine the branching ratio between the two bound X states. Calculations[70] performed on the tripod photoassociation of a wave packet in the $X^1\Sigma_g^+$-continuum to the $X^1\Sigma_g^+(v = 4, J = 0)$ state via the $A^1\Sigma_u^+/b^3\Pi_u(v = 133, J = 1)$ state using an additional dump pulse that couples the same intermediate $A^1\Sigma_u^+/b^3\Pi_u(v = 133, J = 1)$ state to a different final state $X^1\Sigma_g^+(v = 5, J = 0)$, $E = -3944$ cm^{-1}, confirm this expectation: the probability to populate either the $X^1\Sigma_g^+(v = 4, J = 0)$ or $X^1\Sigma_g^+(v = 5, J = 0)$ state is indeed proportional to the corresponding ratio between the Rabi frequencies-squared.

3. EXPERIMENTAL REALIZATIONS: MAGNETOASSOCIATION FOLLOWED BY ADIABATIC PASSAGE

Dark states that arise in the adiabatic passage from the continuum, as discussed above, have been observed experimentally.[43,44,75] Similarly, dark states associated with Feshbach molecules[46,47] have been observed.[45] In Figure 11 we display
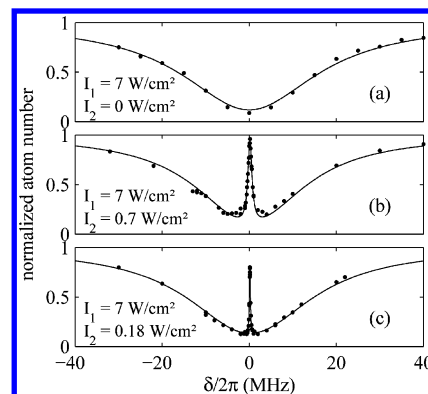

Figure 11. The atomic Rb signal as a function of δ—the detuning from resonance of the pump laser at three different dump laser intensities. (a) Dump intensity = 0. The concentration of the Rb atoms is depleted as a result of photoassociation of two Rb atoms to form a Rb$_2$ molecule as I_1 sweeps through the resonance. For (b) dump intensity = 0.7W/cm^2 and (c) dump intensity = 0.18W/cm^2, a narrow dark state, corresponding to the quenching of the photoassociation and the disappearance of the population in the intermediate molecular level, appears. This dark state becomes narrower and narrower as the intensity of the dump laser goes down. (Compare panel b to panel c.) Reprinted with permission from ref 44. Copyright 2005 American Physical Society.

the results of an experiment measuring the disappearance of the atomic Rb signal due to the photoassociation of Rb atoms to form Rb$_2$ molecules. In this experiment two CW lasers were used, one serving as a pump, and the other as a dump, to photoassociate Rb atoms in a Rb Bose–Einstein condensate to form a degenerate gas of Rb$_2$ ground-state molecules in a specific vib-rotational state. As a signature for the decoupling of this coherent atom-molecule gas from the light field, a striking suppression ("dark state" formation) of photoassociation loss is observed. The experimentally observed dark state is similar to the theoretical one presented in Figure 3 in that the population in the intermediate state in both cases is negligible. In contrast to the theory displayed in Figure 3, the experiment involves CW light fields; hence, no population transfer due to the temporal evolution of this dark state has been observed.

An important tool in performing PA to form ultracold molecules has been the use of "Feshbach molecules" as

I

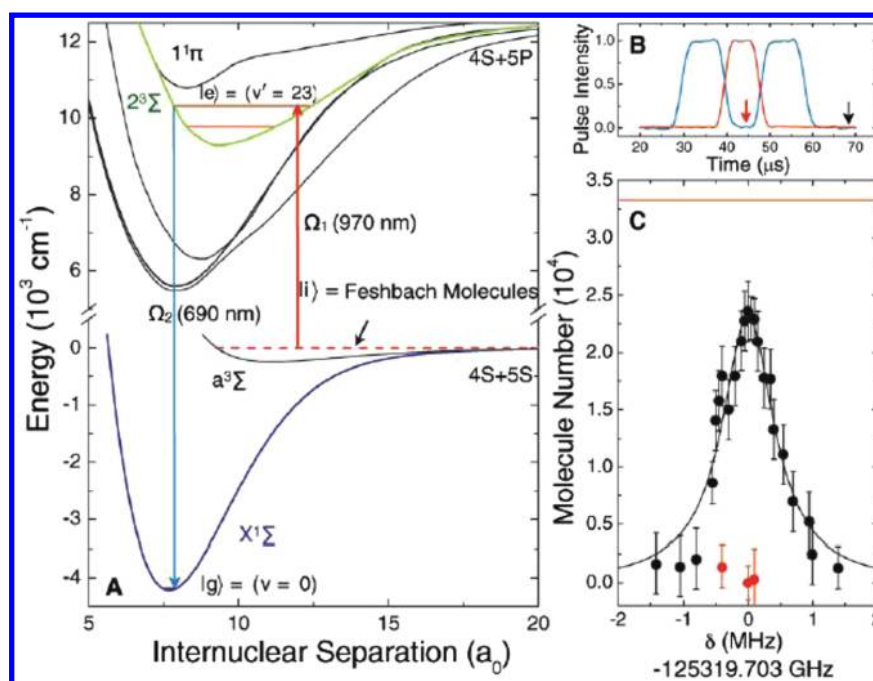dx.doi.org/10.1021/cr2003882 | Chem. Rev. XXXX, XXX, XXX–XXX

Figure 12. Two-photon coherent state transfer from weakly bound Feshbach molecules $|i\rangle$ to the absolute molecular ground state $|g\rangle$ ($v = 0$, $J = 0$ of $X^1\Sigma^+$). (A) Transfer scheme. Here, the intermediate state $|e\rangle$ is the $v' = 23$ level of the $\Omega = 1$ component of the electronically excited $2^3\Sigma^+$ potential. The chosen intermediate state lies just below the $1^1\Pi$ excited electronic potential, which provides the necessary triplet−singlet spin mixing to transfer predominantly triplet character Feshbach molecules to the vib-rotational ground state of the singlet electronic ground potential, $X^1\Sigma^+$. The vertical arrows are placed at the regions of greatest overlap of the up and down transitions. (B) Normalized Raman laser intensities versus time for the round-trip STIRAP pulse sequence. Four transfers were performed each way using a maximum Rabi frequency of $2\pi \times 7$ MHz for the downward transition (blue line) and a maximum Rabi frequency of $2\pi \times 4$ MHz for the upward transition (red line). (C) The number of Feshbach molecules recovered after a round-trip STIRAP transfer is plotted as a function of the detuning from a two-photon resonance. The round-trip data were taken at the time indicated by the black arrow in part B. The red data points show the remaining Feshbach molecule number when only one-way STIRAP is performed (at the time indicated by the red arrow in part B), where all Feshbach molecules are transferred to the ground state and are dark to the imaging light. The initial Feshbach molecule number is $3.3(4) \times 10^4$ (red solid line), and the number after round-trip STIRAP is 2.3×10^4. The round-trip efficiency is 69%, which suggests the one-way transfer efficiency is 83% and the number of the absolute ground-state polar molecules is 2.7 $\times 10^4$. Reprinted with permission from ref 45. Copyright 2008 AAAS.

intermediates. A Feshbach molecule[46,47,76] is a scattering resonance whose center energy is tuned magnetically to lie *below* the molecular dissociation limit. Feshbach molecules are bound states, but because of their very weak binding energy, they usually dissociate upon collisions with other atoms or molecules. Photoassociation to form ultracold ground state molecules using "Feshbach molecules" as intermediates has been demonstrated by a number of groups.[45,48,51,52] Winkler et al.[48] have used this technique to create ground state $^{87}\text{Rb}_2$ molecules, Ni et al.[45] have created $^{40}\text{K}^{87}\text{Rb}$ heteronuclear molecules, and Spiegelhalder et al.[52] have created an ensemble of $^6\text{Li}^{40}\text{K}$. In all these experiments, one makes use of a STIRAP process (see Figure 12) to coherently transfer the extremely weakly bound $^{87}\text{Rb}_2$ or KRb Feshbach molecules to the vib-rotational ground state of the ground electronic state.

The KRb experiment[45] was remarkable in being able to produce an ensemble of molecules at relatively high density ($n = 10^{12}$ cm^{-3}) at an (expansion-determined) translational temperature of 350 nK. The starting point of this experiment was an atomic degenerate gas mixture of fermionic ^{40}K atoms and bosonic ^{87}Rb atoms confined in an optical dipole trap. By using a 550G magnetic field, it was possible to lower the energy of a Feshbach resonance lying above the onset of the continuum to a truly bound state.[77−80] As many as 10^4 Feshbach molecules, whose binding energy of 0.767×10^{-5} cm^{-1} can be detected directly using time-of-flight absorption imaging, were thus formed.

As shown in Figure 12A, the transfer scheme of the Feshbach molecules to a$^3\Sigma^+$ $v = 0$ molecules involves three molecular levels, the initial state $|i\rangle$, the intermediate state $|e\rangle$, and the final state $|g\rangle$. These states are coupled by two laser fields. The pump laser drives the up transition to the $|e\rangle = |v' = 23\rangle$ vibrational level of the electronically excited $2^3\Sigma^+$ state. This state has good FC overlaps with both the weakly bound Feshbach molecule and the deeply bound ground vibrational state $|g\rangle$, which is coupled to it by the dump laser field. As shown in Figure 12A, the main contribution to the $\langle e|i\rangle$ FC integral occurs near the outer turning point of $|e\rangle$, whereas the $\langle g|e\rangle$ FC integral borrows its strength from the good overlap in the inner turning point region of $|e\rangle$.

In Figure 12B we see typical time profiles of the pump and dump pulses for a full *round trip* composed of two STIRAP processes: The first process, corresponding to the $|i\rangle \rightarrow |e\rangle$ transfer, is followed after some delay by a process demonstrating good recovery of population in which the opposite $|e\rangle \rightarrow |i\rangle$ transfer is executed. True to the "counterintuitive" pulse ordering of STIRAP,[53] the dump pulse precedes the pump pulse in the $|i\rangle \rightarrow |e\rangle$ transfer, with a reverse order in the $|e\rangle \rightarrow |i\rangle$ transfer. Figure 12C displays the number of Feshbach molecules recovered after one round-trip STIRAP transfer as a function of the detuning from the two-photon resonance. The initial number of Feshbach molecules is $3.3(4) \times 10^4$ (red solid line), and the number after an on-resonance round-trip STIRAP is 2.3×10^4. The round-trip

efficiency is thus 69%, suggesting that the one-way transfer efficiency is 83% and the number of the absolute ground-state polar molecules is 2.7×10^4.

The above picture is supplemented in Figure 13A, taken also from ref 45, which displays the number of remaining Feshbach
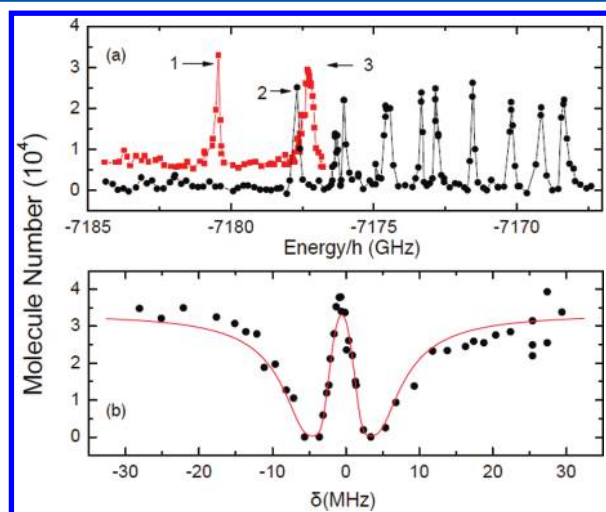

Figure 13. The $v = 0$ ground-state level of the triplet electronic ground potential, $a^3\Sigma^+$. (A) Hyperfine and rotational states of the $a^3\Sigma^+$ $v = 0$ ground-state molecule at a magnetic field of 546.94 G, observed using two-photon spectroscopy and scanning the frequency of the dump field. The measured number of remaining Feshbach molecules is plotted as a function of the frequency difference of the two laser fields. Shown are two sets of data, vertically offset for clarity, obtained using two different intermediate states, which are the hyperfine and rotational states of the $v' = 10$ level of the electronically excited $2^3\Sigma^+$ potential. Peaks labeled 1 and 2 correspond to hyperfine states in the rotational ground-state, and peak 3 corresponds to a rotationally excited state. (B) A precise determination of the energy and the transition dipole moments for individual states using the two-photon spectroscopy by scanning the up leg Ω_1 frequency. The measured number of remaining Feshbach molecules is plotted as a function of the two-photon detuning. The dark resonance shown here is for the triplet vib-rotational ground state corresponding to peak 2 in part A. Reprinted with permission from ref 45. Copyright 2008 AAAS.

molecules as a function of the pump and dump frequency difference. Figure 13B demonstrates the decoupling of the system from the laser fields and the formation of a dark state involving a Feshbach molecule as the dump laser is scanned across one of the two-photon resonances shown in Figure 13A.

The above experiments clearly show that the field of photoassociation of ultracold atoms to form ultracold molecules analyzed theoretically above has reached a maturity which would enable the production of ultracold molecules in large densities as a preparatory step for performing coherently controlled bimolecular reactions.[81−84]

4. PUMP−DUMP PHOTOASSOCIATION WITH SHORT LASER PULSES

An alternative approach to adiabatic passage employs laser pulses for photoassociation that are shorter than the vibrational period of the trap and any other relevant dynamical time scale. The natural choice to probe the photoassociation dynamics of ultracold atoms is the picosecond time scale.[85] An initial pulse, the "photoassociation" or "pump" pulse, creates a vibrational wave packet in the electronically excited state, close to the outer

classical turning point.[35] Squeezed by the excited state potential, the wave packet travels toward shorter internuclear distances. The shape of the long-range part of the excited state potentials, that scales as some inverse power of the internuclear distance R, suggests plausible pulse shapes, such as linear chirps that ensure spatial focusing of the wave packet at the inner turning point.[36,37] Once the wave packet has reached its inner turning point, a second pulse, the "stabilization" or "dump" pulse, transfers it back to the electronic ground state.

The above nonadiabatic photoassication scheme employing a pump−dump process[38−41] is visualized in Figure 14.
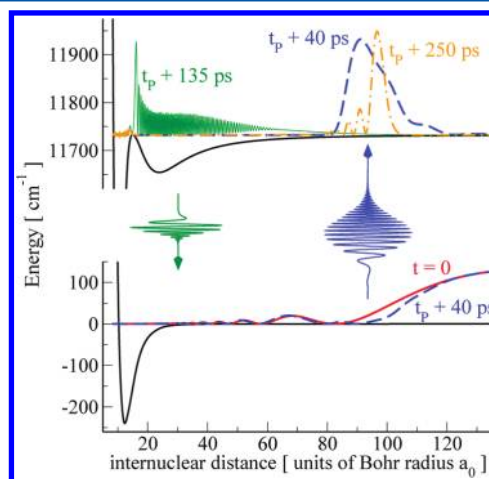

Figure 14. Pump−dump photoassociation with chirped picosecond laser pulses: A photoassociation pulse, shown in blue, excites a small part of the pair density of atoms colliding in their electronic ground state to an electronically excited state (here the Cs_2 $0_g^-(6s6p_{3/2})$ state). A vibrational wavepacket is created (dashed blue line) which travels toward shorter internuclear distances under the influence of the excited state potential. After half a vibrational period, it reaches its inner turning point (green line). A suitable chirp of the photo-association pulse ensures optimum spatial focusing of the wavepacket at its inner turning point. A stabilization pulse, shown in green, dumps the wavepacket to the electronic ground state. Reprinted with permission from ref 38. Copyright 2006 American Physical Society.

When two electronic states are involved, we obtain, invoking the rotating wave approximation, a description of the process by the Hamiltonian

$$H = \begin{pmatrix} T + V_g(R) & \varepsilon^*(t)\, d(R) \\ \varepsilon(t)\, d(R) & T + V_e(R) - \hbar\omega_L \end{pmatrix} \quad (52)$$

Here T and $V_{g/e}(R)$ denote the kinetic and potential energy, and $d(R)$ is the transition dipole moment. The laser pulse is characterized by its central frequency, ω_L, and by a slowly varying envelope, assumed to be Gaussian, $\varepsilon(t) = \varepsilon_0 e^{((t-t_0)^2/(2\sigma^2))} e^{i/2\chi(t-t_0)^2}$, with ε_0 being the peak field amplitude. The width, σ, is related to the full width at half-maximum of the intensity profile, τ, by $\sigma = \tau/2(\ln 2)^{1/2}$. The parameter χ controls the linear chirp rate. The following subsections discuss how to choose the pulse parameters.

The sequence of photoassociation and stabilization pulses needs to be repeated many times because a single photo-association pulse can address only the (small) fraction of atoms whose interatomic distances R are sufficiently close to the Condon radius, R_L, defined by the resonance condition for the

K

dx.doi.org/10.1021/cr2003882 | *Chem. Rev.* XXXX, XXX, XXX−XXX

central laser frequency. To accumulate the photoassociated molecules, the coherent pump–dump sequence must be combined with a dissipative step to ensure that molecules photoassociated by the first pump–dump pair of pulses will not be dissociated by the pulses that follow it.[40] Photoassociation with pairs of short laser pulses is therefore best suited to ultracold temperatures, $T < 1$ mK, but well above the quantum degenerate gas regime.[86]

In the ultracold temperature regime, the scattering energy of a pair of atoms is much smaller than their potential energy for a large range of interatomic distances, extending to $R \approx 100a_0$ and beyond. This threshold behavior[87] is manifest in a distinct nodal structure at short and intermediate interatomic distances of the thermal gas probability density; see, e.g., Figure 15. It is
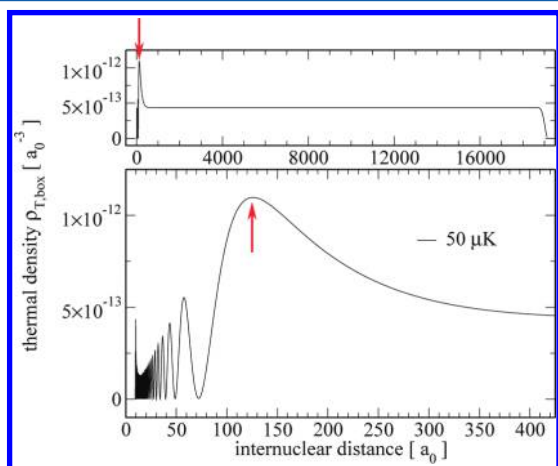

Figure 15. Probability density for a thermal ensemble of ^{87}Rb atom pairs, obtained by incoherently summing over all Boltzmann-weighted scattering wave functions.[88] The red arrow indicates the choice of Condon radius resulting in the largest number of photoassociated molecules per pulse, which is limited by the density of ground state atom pairs. It corresponds to the position of the outermost peak of the last bound ground state level. The thermal density calculated from wave functions normalized to unity in a large box can easily be converted into photoassociation rates by converting to energy normalization.[37,88,89] Figure adapted from ref 88.

derived in the framework of the canonical ensemble, $\rho_T = 1/Z e^{-H_g/k_B T}$, using a large Fourier grid,[88]

$$\rho_T(R) = \frac{1}{4\pi R^2} \frac{\sum_{nl}(2l+1)e^{-E_{nl}/k_B T}|\varphi_{nl}(R)|^2}{\sum_{nl}(2l+1)e^{-E_{nl}/k_B T}} \qquad (53)$$

where E_{nl} denotes the energy eigenvalues for partial wave l of the ground state Hamiltonian,

$$H_l = T + \hbar l(l+1)/2mR^2 + V_g(R)$$

with $\varphi_{nl}(R)$ being the corresponding scattering wave functions.[90]

The intricate small distance nodal structure is distinct from the constant probability of finding two atoms at large interatomic separations R. It is determined by the zeroes of the scattering wave functions within the small band of thermally populated energies that contribute to the incoherent sum of the thermal ensemble.[88] The positions of these zeros, determined by (anti-) correlations of the atom pairs, dictate the choice of the central frequency (or detuning from the atomic line) and the spectral width of the photoassociation pulse.

4.1. Choosing the Pulse Durations and Bandwidths

In the simplest implementation of the pump–dump sequence, a wave packet excited by absorbing a single photon from the pump pulse, traveling for half a vibrational period from the outer to the inner turning point, is dumped onto the electronic ground state by a second pulse; cf. Figure 14. The vibrational level spacing of the electronically excited state sets a lower limit to the spectral width and, hence, an upper limit to the duration of the (transform-limited) pulse: The spectral width of the pulses needs to be much larger than the vibrational level spacing in the excited state. This ensures that several vibrational levels are excited by the pulse and that their superposition yields a localized time-dependent wave packet.[41] Such a requirement on the spectral width translates into pulse durations of the order of 10 ps.[35–38,41] There is also an upper limit to the spectral bandwidth (translating to a lower limit on the pulse duration),[39] which stems from the requirement that the pulse should not contain spectral regions leading to single atoms excitations and loss of atoms from the trap. However, photoassociation transitions are most efficient very close to the atomic resonance where the free-bound Franck–Condon factors are the largest. This is evident from the inspection of the pair density of scattering atoms, which is largest at interatomic separations of 50–200a_0; cf. Figure 15. The compromise of exciting as close as possible to the atomic resonance without actually hitting it translates into narrow-band pulses with a spectral width of a few inverse centimeters or (transform-limited) pulse durations of a few picoseconds.[39]

In such settings, the broad bandwidth of femtosecond laser pulses is more of an obstacle than an asset. Thus, the first experiments aimed at femtosecond photoassociation have resulted in the destruction of the sample of ultracold atoms rather than in forming molecules.[39,91,92] The broad spectral widths of femtosecond pulses are beneficial when we make use of nonresonant multiphoton transitions[93] where optical interference can render the transition of single atoms dark. Specifically, phase shaped pulses containing a properly placed π-jump in the spectral phase function can lead to the destructive interference between two-photon-pairs, thereby suppressing all the two-photon atomic absorptions.[94,95]

Applying such coherent control concepts to photoassociation with weak femtosecond laser pulses, one finds that while atomic excitations and photoassociation into the very last bound levels are suppressed, levels with sufficient binding energy are excited; see Figure 16a. After deexcitation to the electronic ground state, only levels with sufficient binding energy yield molecules while the last bound levels are predominantly redissociated. Phase shaping of two-photon femtosecond photoassociation is thus a viable control scheme in the weak-field regime, allowing formation of deeply bound molecular levels while keeping the atomic transitions dark. It is straightforward to extend this control scheme to higher-order multiphoton transitions, allowing for electronic states with a long-range behavior better suited for photoassociation, or strong nonadiabatic couplings which cause stabilization to the ground state, to be accessed.

For higher pulse energies, the dynamical Stark shift,

$$\omega_{g/e}^S = -\frac{1}{2}\varepsilon_0^2 |S(t)|^2 \sum_m \frac{|d_{m(g/e)}|^2 \omega_{m(g/e)}}{\omega_{m(g/e)}^2 - \omega_L^2}$$

due to off-resonant one-photon transitions to levels m, may become so large that the destructive optical interference of all two-photon pairs, which is intimately linked to the field-free
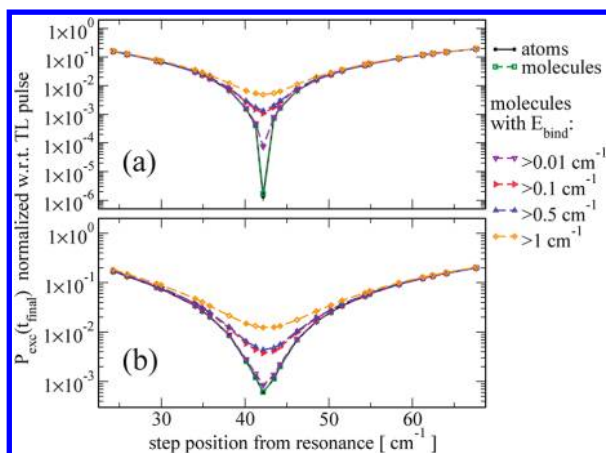
Figure 16. Weak-field control of two-photon femtosecond photo-association at the $^1S + ^1D$ dissociation threshold of $^{40}Ca_2$ using phase-shaped pulses of 100 fs transform-limited duration and a central frequency of 915 nm. (a) Weak field regime ($\mathcal{E}_P = 0.94\ \mu J$): Excitation of single atoms by the femtosecond pulses can be suppressed by 6 orders of magnitude using optical interference in the two-photon absorption.[94,95] Photoassociation into the last bound levels is equally suppressed, but levels with sufficient binding energy ($E_{bind} > 1\ cm^{-1}$) can be excited. It it those levels which are relevant for molecule formation, since deexcitation from these levels populates bound levels of the electronic ground state rather than to redissociate the molecules. (b) Intermediate field regime ($\mathcal{E}_P = 2.4\ \mu J$): The dynamical Stark shift moves the levels out of resonance. A pure frequency-domain picture is not valid anymore, since the condition for destructive optical interference cannot be defined. The weak-field control scheme thus ceases to work, and excitation of single atoms is suppressed by only 3 orders of magnitude. Reprinted with permission from ref 93. Copyright 2009 The Royal Society of Chemistry.

resonance condition, can no longer be expected to hold. This effect is illustrated in Figure 16b, where the excitation of single atoms is suppressed by only 3 orders of magnitude for an intermediate pulse energy, compared to suppression by 6 orders of magnitude for weak pulses. At even larger pulse energies, single atoms are strongly excited despite the phase shaping of the pulses.[94,95]

In the strong field regime it is possible to control atomic absorption by chirping the pulses to compensate for the dynamical Stark shift. In this way one controls population transfer by effectively controlling the two-photon Rabi flopping process.[96,97] When applied to femtosecond photoassociation, this control scheme does not, however, distinguish sufficiently between atoms and weakly bound molecules. For example, forcing atoms to undergo a two-photon 2π transition also suppresses their photoassociation.[98]

4.2. Optimizing the Pump Step by Controlling a Scattering Resonance

Photoassociation can easily be saturated: A pulse energy of only a few nano-Joule is typically sufficient to completely deplete the pair density within the "photoassociation window", i.e., the range of internuclear separations for which the pulse induces a resonant excitation; see Figure 17.[99] As discussed in section 2.4 (see Figure 9), the number of molecules that can be photoassociated per pulse is limited by the pulse duration and the density of atom pairs within the photoassociation window.[39] Even for optimally chosen parameters of the photoassociation pulse, only a few molecules can be photo-associated per pump—dump sequence.[88]
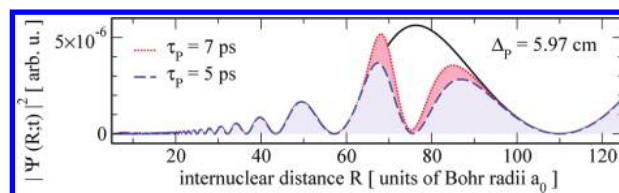

Figure 17. Ground state scattering wave function of a ^{87}Rb atom pair before (solid black line) and after (dashed blue and dotted red lines) the photoassociation pulse: Around the Condon radius, within the "photoassociation window" defined by the spectral width of the pulse, a hole is carved into the ground state probability density. τ_P is the pulse duration, Δ_P is the detuning from the atomic D_1 line, and the pulse energy amounts to 4.2 nJ. Reprinted with permission from ref 39. Copyright 2006 American Physical Society.

Before sending the next photoassociation pulse, a sufficient time needs to elapse to allow for refilling the photoassociation hole. Otherwise, the second photoassociation pulse will find an even smaller pair density and create less molecules than the first one. However, equilibration of the ultracold gas proceeds very slowly, such that the overall photoassociation rate remains very small. It therefore seems expedient to manipulate the thermal gas of atoms prior to photoassociation in order to enhance the pair density at interatomic separations amenable to photo-association.

Controlling the continuum of scattering atoms is a highly nontrivial task. In general, it represents a problem which is, in mathematical terms, not controllable. This situation changes only in the presence of resonances which endow the otherwise flat continuum with a sharp structure.[100] Scattering resonances are well-known to enhance the density of atom pairs at short and intermediate distances. Therefore, the presence of a Feshbach resonance has been predicted to significantly enhance the photoassociation yield in Feshbach optimized photo-association (FOPA).[101,102] However, Feshbach enhancement of photoassociation is restricted to atoms with a hyperfine manifold and is most efficient at temperatures in the nano-Kelvin range. Electric field-induced resonances[103−105] should also increase the photoassociation efficiency. The electric fields required to achieve a significant enhancement are, however, not within present day experimental feasibility.

Another type of resonance occurs when a scattering state becomes trapped behind the centrifugal barrier, occurring naturally for $l > 0$ partial waves. Such "shape" resonances were found to yield enhanced photoassociation rates.[106−108] However, because the barriers are generated at $l > 0$ partial waves, the lowest temperatures at which shape resonances typically occur are in the milli-Kelvin regime. Therefore, the thermal weight of a shape resonance in much colder traps is quite small.

It is possible to enhance the pair density at internuclear distances relevant for photoassociation using nonresonant light.[109] The interaction of nonresonant light with the polarizability anisotropy of the atom pair, as described by the Hamiltonian,

$$H^I = T_R + \frac{l^2}{2\mu R^2} + V_g(R) - \frac{2\pi I}{c}(\Delta\alpha(R)\cos^2\theta + \alpha_\perp(R)) \tag{54}$$

moves the position of the shape resonances closer to the trap temperature. By adiabatically separating vibrational and rotational motion, it is possible to see how nonresonant light affects

M

dx.doi.org/10.1021/cr2003882 | Chem. Rev. XXXX, XXX, XXX−XXX

the height of the rotational barrier and the position of the shape resonance.[109] This effect is illustrated in Figure 18. It is found
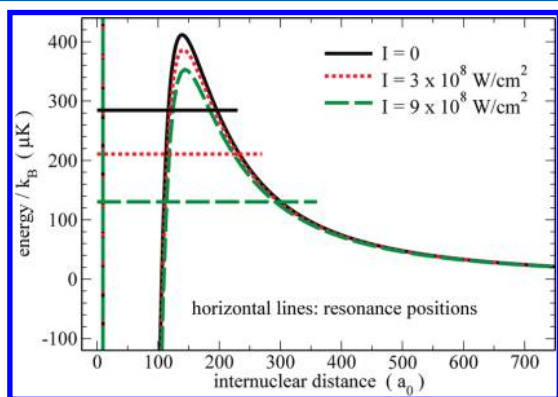

Figure 18. Effective potential, $V_g(R) + E_1(R;I)$, that an atom pair experiences in the presence of nonresonant laser light, shown here for the field-free l = 2 shape resonance at about 290 μK of ^{87}Rb$_2$. The position of the shape resonance is indicated by the horizontal lines for three values of the nonresonant light intensity.[109]

that to shift the shape resonance closer to the trap temperature, nonresonant field intensities of the order of 10^8–10^9 W/cm^2 are required, with the exact value depending on the initial position of the resonance, the polarizability of the atom, and the trap temperature.

Figure 19 demonstrates for the example of ^{87}Rb atoms that application of nonresonant light indeed leads to an enhanced
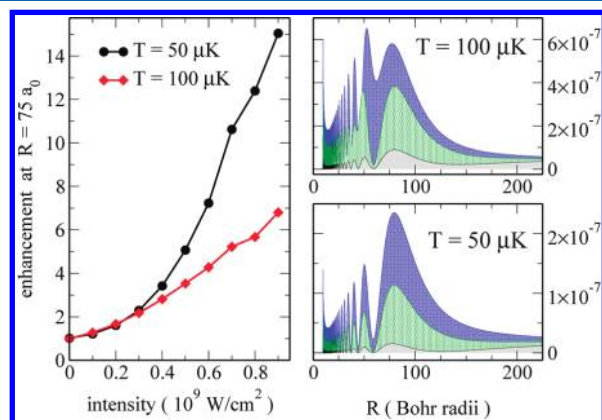

Figure 19. Modification of the pair density: Enhancement near a Condon radius of $R = 75a_0$ (left) and R-dependence of the field-dressed pair density, cf. eq 53, for zero field (gray), $I = 0.6 \times 10^9$ W/cm^2 (green), and $I = 0.9 \times 10^9$ W/cm^2 (blue), assuming ^{87}Rb atoms held at the temperatures 50 μK and 100 μK, respectively.[109]

pair density at interatomic separations where photoassociation is most efficient. The enhancement is significantly larger for a trap temperature of 50 μK compared to $T = 100$ μK. This is due to the fact that, for rubidium, the lowest shape resonance occurs at $E_{res}/k_B \approx 290$ μK, much lower than for most species. At a trap temperature of $T = 100$ μK, the resonance has already perceivable thermal weight without applying a nonresonant field.[88] At $T = 50$ μK, the field-free thermal weight of the resonance is much smaller and the enhancement subsequently larger. The thermal pair density, shown on the right-hand side of Figure 19, is obtained as the Boltzmann-weighted sum over all field-dressed scattering states. For large intensities of the

nonresonant field, the oscillations in the short-range part of the pair density cease to pass through zero, indicating the admixture of partial waves with l > 0.

The pair density enhancement at short interatomic separations predicted by Figure 19 can be realized by slowly ramping the nonresonant field up until the desired intensity is reached such that the thermal cloud of atoms follows adiabatically. The modified pair density is then subjected to photoassociation, either nonadiabatically by a pump–dump sequence or by using adiabatic passage, as described above. This requires, however, that the lifetime of the resonance is sufficiently long to allow for adiabatic following and subsequent photoassociation. Otherwise, the atom pairs will have tunneled out of the rotational barrier, disappearing from the photo-association window before they are excited by the pump pulse or have lost their well-defined phase by the time the adiabatic passage starts. It appears that an adiabatic ramp of the nonresonant field followed by a pump–dump sequence of picosecond pulses should be feasible. However, it is not straightforward to predict the lifetime of the field-dressed resonance, since it strongly depends on the degree of hybridization and the presence and character of further shape resonances.

As an alternative method, the pump–dump photoassociation yield may be increased using a method called "flux enhancement". In "flux enhancement" the atom pair density at short interatomic separations is increased by performing a preliminary excitation of atom pairs by a chirped nanosecond laser pulse tuned very close to the atomic resonance.[110,111] As the atom pair rolls down the potential curve of the electronically excited state toward shorter interatomic distances, a vertical down transition back to the electronic ground state may occur, either due to the pulse or by spontaneous emission. Though the atom pair will have gained some kinetic energy in the process, it is not enough to leave the trap. Thus, by placing in this manner the atom pairs at shorter interatomic distances, the yield of the pulsed photoassociation process is expected to be greatly increased. Picosecond pulses are also expected to lead to flux enhancement.[112−114]

4.3. Optimizing the Dump Step: Vibrational Structure and Franck−Condon Engineering

Having discussed the optimal pump pulse parameters, we now discuss the optimization of the dump step in which the electronically excited molecules are stabilized to form ground state molecules. In principle, optimal control can transfer any coherent state, however weakly bound, into the absolute ground state with a transfer efficiency of close to one hundred percent.[98] In a brute force approach, this requires, however, very strong fields that drive many Rabi cycles and can lead to undesired effects such as autoionization or predissociation. It is therefore useful to build the control upon a thourough analysis of the pathways associated with large bound−bound Franck−Condon factors.

Regular potentials of an electronically excited state, in particular those with $1/R^3$ long-range behavior yielding the best free−bound Franck−Condon factors for photoassociation, are not well suited for the formation of molecules in their electronic ground state. In CW-photoassociation, spontaneous emission will simply redissociate most of the molecules formed in such a state.[19,21] Analogously, a transform-limited dump or stabilization pulse can transfer only a very small part of these molecules into bound levels in the electronic ground state,

N

dx.doi.org/10.1021/cr2003882 | Chem. Rev. XXXX, XXX, XXX–XXX

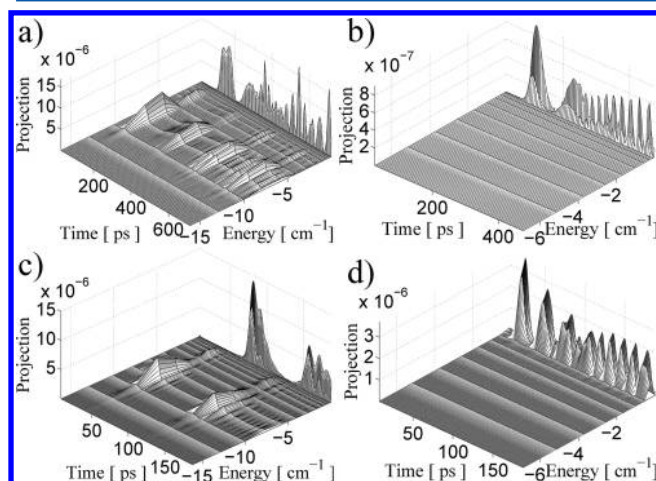predominantly into the very last bound levels.[39] This is illustrated in Figure 20b and d.

Figure 20. Time-dependent transition matrix elements vs time and binding energy in the electronic ground state for ^{87}Rb$_2$ after excitation to the electronically excited states 0^+_u (a, c), 1_g (b), and 0^-_g (d) with photoassociation laser detuning $\Delta\omega_P = 4.1$ cm^{-1} (a, b) and $\Delta\omega_P = 8.6$ cm^{-1} (c, d). Deexcitation from regular states (1_g and 0^-_g, b + d) can populate only the very last bound levels of the electronic ground state, while resonant coupling due to strong spin−orbit interaction (0^+_u, a + c) allows for transitions into more deeply bound ground state levels. Reprinted with permission from ref 39. Copyright 2006 American Physical Society.

The excited state potential curve may, however, exhibit properties which make it suitable for ground state molecule formation. The most prominent examples discussed in the literature are a double-well shape of the potential[17] and resonant coupling of two electronic states.[19] Both features are present in heavy alkali dimers due to strong spin−orbit interaction. A double well such as that found in the Cs$_2$ 0^-_g(6s + 6p$_{3/2}$) state has two effects that are favorable for stabilization: A wave packet is created at the outer turning point of the outer well. It is slowed down by the softly repulsive wall ($\sim -1/R^3$) near the inner turning point of the outer well. This leads to a wavepacket which resides close to the inner turning with a piled up probability amplitude for a sufficient amount of time such that it can be captured by the dump pulse,[38] cf. Figure 14. Without any specific optimization of the dump pulse, about 20% of the excited state wave packet are transferred to vibrational levels bound by about 100 cm^{-1} in the lowest triplet state of Cs$_2$.[38] The excited state wave packet may also tunnel through the barrier into the inner well, which allows for stabilization into deeply bound levels of the electronic ground state.[10]

The coupling of two electronic states due to spin−orbit interaction may become resonant if the corresponding potential energy curves cross at short interatomic distances. The two vibrational ladders are then mixed. Whenever two vibrational levels are close in energy, their wave functions are strongly perturbed, and each diabatic component shows peaks at all four classical turning points of the two potentials. The perturbed wave functions are readily identified experimentally by inspection of the rotational constants.[115,116] The distinct nodal structure of the perturbed wave functions leads to significantly enhanced bound−bound Franck−Condon factors, in particular for very weakly bound excited state levels.[19,115] As

shown in Figure 20a and c for the example of ^{87}Rb$_2$ 0^+_u(5s + 5p$_{1/2}$), the enhanced Franck−Condon factors can be exploited by the dump pulse. The corresponding Hamiltonian reads

$$H_3 = \begin{pmatrix} T + V_{X^1\Sigma^+_g}(R) & d(R)\,\varepsilon(t) & 0 \\ d(R)\,\varepsilon(t) & T + V_{A^1\Sigma^+_u}(R) - \hbar\omega_L & \sqrt{2}\,W^{od}_{SO}(R) \\ 0 & \sqrt{2}\,W^{od}_{SO}(R) & T + V_{b^3\Pi_u}(R) - W^d_{SO}(R) - \hbar\omega_L \end{pmatrix}$$
(55)

where $W^d_{SO}(R)$ and $W^{od}_{SO}(R)$ denote the diagonal and off-diagonal coupling due to spin−orbit interaction, respectively. Solving the time-dependent Schrödinger equation for the dump pulse, population of ground state levels with significantly larger binding energy than those obtained from photoassociation into regular states is obtained.[39] Up to 50% of the excited state molecules can be transferred into a coherent superposition of bound ground state levels, and up to 20% into a single ground state level for sufficiently intense dump pulses.[39] This efficiency is actually higher than that predicted by the Franck−Condon factors and is due to a dynamical interplay between the dump pulse and the spin−orbit coupling: The electronically excited molecules have components on two electronic states (the $A^1\Sigma^+_u$ and $b^3\Pi_u$ states), but only the singlet component is coupled to the electronic ground state by the field. When the dump pulse acts, the singlet component is depleted by the pulse, but it is "refilled" by the resonant spin−orbit coupling. Thus, significantly more population is channeled to the ground state than expected from the bound−bound Franck−Condon factors, which only account for the singlet component.

The case of ^{87}Rb$_2$ 0^+_u(5s + 5p$_{1/2}$) is particularly well suited for pump−dump photoassociation, since one always finds several strongly perturbed levels close to each other. The detuning and spectral width of the photoassociation pulse can then be chosen such that exclusively perturbed levels are populated. In heavy heteronuclear dimers such as RbCs or SrYb, only single levels are found that display resonantly perturbed wave functions.[117,118] The contribution of the single resonantly perturbed level to a coherent wavepacket can then be efficiently dumped to the electronic ground state. This drawback is compensated by the fact that, for heteronuclear molecules, the peak at the inner classical turning point of the singlet state is much larger than that for the homonuclear molecules. The reason for this is that Rb$_2$ has an $1/R^3$ potential at long-range, and the vibrational wave functions of states near the dissociation threshold are more strongly concentrated at the outer turning point.[117] The strong peak at the inner classical turning point of the singlet state for heteronuclear molecules allows for stabilization about halfway down the electronic ground state potential in the case of RbCs[117] and all the way down to $v'' = 0$ or 1 for SrYb.[118]

It is natural to ask what chances one has to transfer molecules to levels deep in the potential well of the electronic ground state if no double-well or resonantly coupled excited states are present in one's molecule of choice. Taking the coherent control idea of shaping the potential energy curves literally, one may use an additional laser field to induce a coupling between two otherwise isolated excited-state potentials.[40] This is described by the generic Hamiltonian

$$H_{\text{gen}} = \begin{pmatrix} T + V_{\text{g}}(R) & d_1\varepsilon(t) & 0 \\ d_1\varepsilon^*(t) & T + V_{\text{e}}(R) & d_2\varepsilon(t) \\ 0 & d_2\varepsilon^*(t) & T + V_{\text{aux}}(R) \end{pmatrix} \tag{56}$$

where $\varepsilon(t)$ is the electric field of both pump/dump and coupling lasers, $\varepsilon(t) = \varepsilon_{0,1}S_1(t)\cos(\omega_1 t) + \varepsilon_{0,2}S_2(t)\cos(\omega_2 t)$. The pump and dump pulses can be considered separately (with $\varepsilon_1(t)$ corresponding to either one of them), since wavepacket propagation in the excited state is slow and the time delay between pump and dump pulses is correspondingly long. In the two-color rotating-wave approximation, $\varepsilon_1(t)$ couples only to d_1, and $\varepsilon_2(t)$ only to d_2. Figure 21 illustrates pump–dump
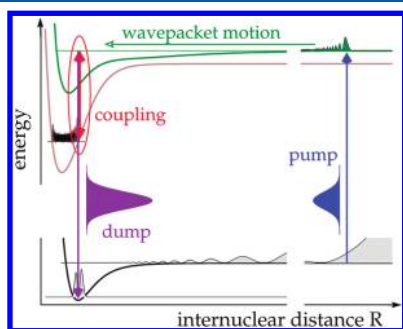

Figure 21. Engineering resonant coupling between two otherwise isolated electronically excited states using an infrared coupling laser, shown here for photoassociation of ^{40}Ca$_2$ molecules. The coupling field is constant on the time scale of the pump–dump photoassociation. This is achieved by a nanosecond pulse. The frequency of the coupling laser determines which target level in the electronic ground state can be reached, for example 881 nm to reach $v'' = 1$. In the frame rotating with the coupling laser frequency, the coupled electronically excited states cross at short interatomic separation, analogously to states coupled resonantly by the spin–orbit interaction. Reprinted with permission from ref 40. Copyright 2008 American Physical Society.

photoassociation employing field-induced resonant coupling. The idea is to mimic the resonant coupling due to spin–orbit interaction by an infrared laser field and thus engineer the bound–bound Franck–Condon factors. A coupling that is constant on the time scale of the pump–dump photoassociation is achieved by employing a nanosecond pulse.[40] The coupling is strong enough to become resonant for couplings larger than the spacing between vibrational levels. This is the case for spin–orbit coupling in heavy alkali dimers (for example 238 cm^{-1} in the first electronically excited state of Rb$_2$). Translating this requirement directly to field-induced resonant coupling would lead to unrealistically large intensities. However, the resonant coupling needs to be engineered only for the weakly bound levels accessed by the photoassociation pulse, not for all vibrational levels. Binding energies of only a few inverse centimeters require intensities of the order of 10^9 W/cm^2 for the nanosecond pulse, which is well within experimental feasibility. The field-induced resonant coupling comes with the advantage, compared to resonant spin–orbit coupling, that the crossing point of the two potentials can be tuned by suitable choice of the coupling laser frequency. One can therefore also control which target level in the electronic ground state is accessed; see Figure 21. It is best to choose the coupling frequency such that $v'' = 1$ instead of the vibronic ground state is targeted. One can then accumulate ground state

molecules by repeatedly forming molecules with $v'' = 1$ and waiting for collisional decay to take them to the ground state. The latter represents the dissipative element required to render the molecule formation scheme unidirectional, as discussed above.

4.4. Experimental Demonstration of Femtosecond Photoassociation

We briefly summarize experiments on femtosecond photoassociation of ultracold molecules and their comparison with theory in the following and refer to ref 119 for a more detailed overview. Initial attempts at photoassociation of ultracold atoms using femtosecond laser pulses were hampered by strong trap loss due to pulse frequency components overlapping with the atomic resonance.[91,92] Removing those frequency components from the broad spectrum using a razor knife in the Fourier plane, femtosecond photoassociation of ultracold atoms was demonstrated experimentally.[120−122] A sharp cut in the spectrum translates into laser pulses in the time domain with very long tails. Recording the pump–probe signal as a function of the delay for these spectrally cut pulses, coherent oscillations in the count rate of molecules were observed;[120] see also Figure 22. The frequency of these oscillations was found to depend linearly on the position of the spectral cut. Solving the time-dependent Schrödinger equation with spectrally cut pulses as employed in the experiment, similar coherent oscillations were observed in the population of the electronically excited state.[120,123] In fact, for all cut positions, chirped and unchirped pulses, and red and blue detuning from both the D1 and D2 atomic resonances, excellent agreement between theory and experiment was obtained.[123−125] A few examples for red-detuned, unchirped pulses are presented in Figure 22. The linear dependence on the cut position precludes the coherent oscillations to be caused by the molecular structure, such as vibrations in the electronically excited state potential. Inspection of the vibrational distribution created by the pump pulse reveals that mostly levels out of resonance with the spectrally cut pulse are populated, cf. Figure 3 of ref 123. Moreover, the coherent oscillations were found to be correlated with the relative phase between molecules and field.[120,123] The oscillations thus correspond to coherent transients that are caused by the long pulse tails: The peak of the pulse photoassociates molecules in the electronically excited state, forming a strong transition dipole. Since the field is still present after the main peak due to the long pulse tails, the dipole continues to interact with the laser. This causes Rabi cycling of the photoassociated molecules. The off-resonant population of vibrational levels is then easily rationalized in terms of power broadening.

The significance of these experiments[91,92,120−122] lies in the first successful application of femtosecond laser technology to ultracold gases. However, control of photoassociation of ultracold atoms with short laser pulses still remains an open challenge. In particular, demonstration of coherent vibrational motion in the electronically excited state is required to not only form molecules but also transfer them to deeply bound ground state levels, achieving full control over the photoassociation reaction products. The various theoretical suggestions discussed above together with the demonstration of basic feasibility of short pulse photoassociation represent a starting point for experimental realization of full coherent control of photoassociation.
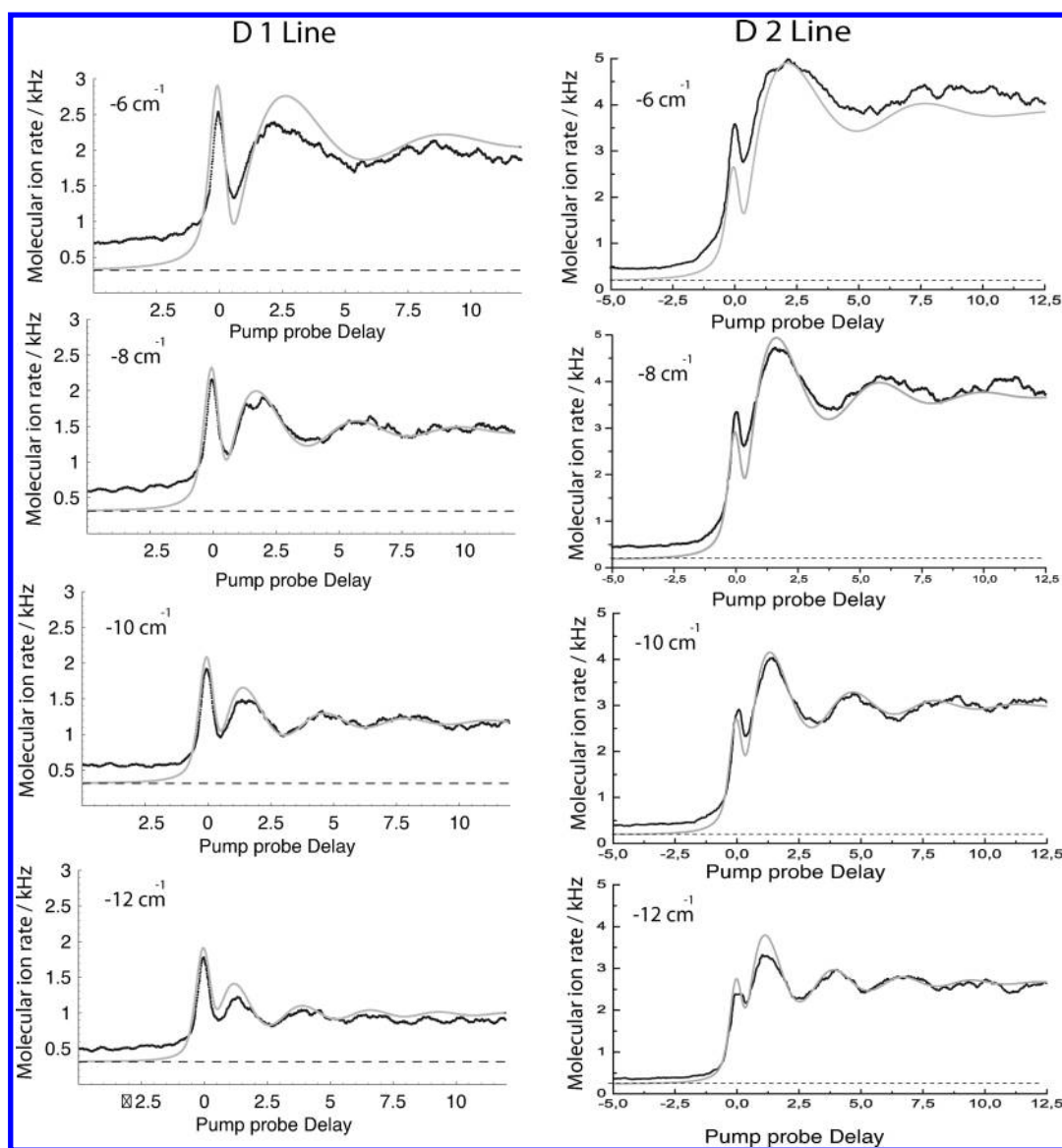
Figure 22. Experimental (black) and theoretical (gray) pump–probe signals for pump pulses with different spectral cutoff positions red to the D1 and D2 line resonances of ^{87}Rb. Reprinted with permission from ref 123. Copyright 2009 American Physical Society.

Another application of femtosecond laser pulses to ultracold gases employs the broad bandwidth of the femtosecond laser for vibrational cooling.[10] That experiment started from photoassociation with CW light followed by spontaneous emission to form an incoherent ensemble of molecules, distributed over many vibrational levels in the electronic ground state. Essentially, vibrational cooling requires broad-band optical pumping for which the vibrational ground state is dark.[6,8,9] Repeated cycles of optical pumping and spontaneous emission will then lead to an accumulation of molecules in the dark state. The dark state requirement was realized experimentally by removing from the pulse spectrum all frequency components that excite the target state.[10] The target level does not need to be the ground state;[126] cooling occurs also if the molecules accumulate in another single level. While the optical pumping can be carried out even with incoherent light,[127] phase shaping of the pulse renders the process more efficient[11] and might become necessary if the Franck–Condon factors are unfavorable.

The broad bandwidth of femtosecond laser pulses can also be used for efficient detection of ground state molecules via resonantly enhanced multiphoton ionization.[128,129] The broad bandwidth simply assures that more molecules are addressed simultaneously than is possible using a narrow band laser.

4.5. Further Prospects: Probing Two-Body Correlations in an Ultracold Gas

The femtosecond photoassociation experiments described in the previous section may pave the way toward a new type of spectroscopy to probe two-body correlations in an ultracold gas.[130,131] Figure 23 illustrates how the many-body pair correlation dynamics can be studied by employing pump–probe spectroscopy originally developed in molecular and chemical physics for an ultracold gas of ^{87}Rb atoms. The pump pulse excites population from the electronic ground to an excited state, leaving a "hole" in the initial pair correlation function. The "hole" represents a nonstationary state that moves under the influence of the ground state potential, cf. Figure 23. The pump pulse thus induces the dynamics of the pair correlations. A time-delayed probe pulse monitors these
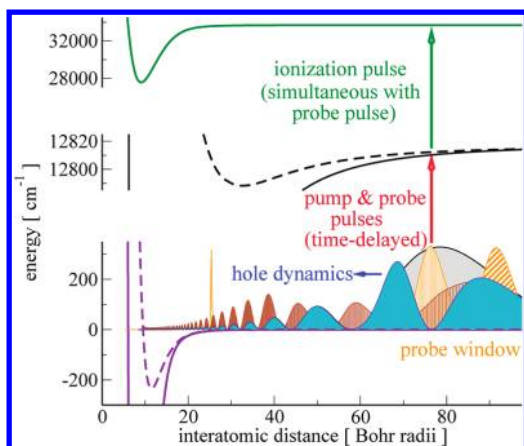
Figure 23. Pump—probe spectroscopy of dynamical pair correlations: A pump pulse excites population from the electronic ground state, leaving the pair correlation function in a nonstationary state, the hole. A time-delayed probe pulse monitors the dynamics of the hole. The orange peaks indicate the region where the probe pulse measures pair amplitude. Reprinted with permission from ref 130. Copyright 2009 American Physical Society.

dynamics by measuring the amount of probability amplitude in a range of internuclear distances. The measurement consists of applying simultaneously a photoassociation and an ionization pulse (combination of red and green arrows in Figure 23). The pair density on the ground state is thus photoassociated and immediately ionized for detection. The largest probe signal is obtained when the probe pulse is identical to the pump pulse. The dynamics are then monitored at the position where the "hole" was created. The spatial region where the probe pulse detects pair density is indicated in orange in Figure 23. Detection of the pair correlation dynamics proceeds via the creation of molecular ions and is inspired by the experiments discussed in the previous section.[120−122] The modification consists in probing the ground state dynamics of the many-body pair correlations.[130] In this setting, photoassociation just serves as a means for detection.

This proposal is based on the fact that the pair correlation dynamics of a dilute, weakly interacting Bose gas can be decoupled from higher-order contributions to the many-body dynamics. Two-body correlations are caused by the microscopic interaction between the particles in an ultracold gas which dictates also the mesoscopic and macroscopic properties of the gas. For dilute gases, the two-body interactions V_2 dominate the dynamics such that the equation of motion for the field operator annihilating (or creating) a particle at position $\vec{x}$ reads

$$i\hbar \frac{\partial \psi}{\partial t}(\vec{x}; t) = H_1 \psi(\vec{x}; t) + \int d^3\vec{y} \; V_2(\vec{x} - \vec{y}) \; \psi^\dagger(\vec{y}; t)$$
$$\psi(\vec{y}; t) \; \psi(\vec{x}; t) \qquad (57)$$

The dynamics of the pair correlations are obtained by expressing the expectation values of the many-body system in terms of normal-ordered correlation functions. Truncating the infinite set of equations of motion for the many-body correlations functions at second order, the dynamics of the pair correlations are decoupled from higher order terms.[130] The truncation is justified by a separation of time or length scales, i.e., small collision time vs long free propagation time or small effective range of the interaction potential vs large interatomic

distance, for dilute Bose gases in a macroscopic trap. The dynamics of the macroscopic pair correlation function is then described by a Schrödinger-like equation where the mean field enters as a source term[132] or acts as an additional potential.[133] If we restrict our considerations to time scales that are much shorter than the time scale of the mean field dynamics, the pair correlation dynamics are described by a standard Schrödinger equation where the presence of the condensate only modifies the boundary conditions.[130] The macroscopic pair correlation function is then given by the two-body wave function of an isolated pair of atoms.

Beyond unraveling the many-body pair correlations in a dilute Bose gas as discussed above, the proposal of ref 130 can be extended to retrieve the pair correlation density operator by performing a tomographic set of measurements, varying the parameters of the probe pulse: The central frequency, ω_P, defines the position that is measured, and the pulse duration, τ_P, controls the resolution. Chirping the probe pulse corresponds to a momentum measurement,[35] required to obtain the phase information.

Existing experimental setups[120−122] need to be only slightly modified to implement this proposal. In particular, transform-limited pulses of about 1 cm^{-1} bandwidth are required for detection of the probe absorption via molecular ions. Spectral features on a scale of less than 1 cm^{-1} can be resolved for pump—probe delays of a few nanoseconds. Pump—probe spectroscopy of the pair correlation dynamics can be employed to capture transient states of ultracold gases such as collapsing condensates or map out the pair correlation function near a resonance despite the finite lifetime of the resonance.

5. CONCLUSIONS

We have reviewed two main aspects of the coherent control of ultracold photoassociation: adiabatic passage and the non-adiabatic pump—dump scheme. In the adiabatic regime, photoassociation is found to proceed via a dark state, analogous to STIRAP for bound states. The continuum of scattering states leads to a source term in the equations of motion of the final state population which is proportional to the pulse amplitude. Though an increase in laser intensity aids the process, the laser intensity cannot be increased beyond a certain limit due to the emergence of back-dissociation. Therefore, an optimal intensity is found whose exact value depends on the pulse duration, given by exact scaling relations.

If the final bound state is the internal ground state or a deeply bound level, it is advantageous to combine photoassociation via adiabatic passage with bound—bound STIRAP because the Franck—Condon factors are then much larger. The bound state populated by adiabatic passage photoassociation then becomes the initial state for bound—bound STIRAP to the desired target state. Such a double-Λ transition circumvents the need for an intermediate level having large Franck—Condon overlap both with the continuum and the final bound state and thus allows for feasible pulse powers. Double-Λ schemes may also be employed to create several pathways for photoassociation which can be interfered coherently.

In the nonadiabatic regime, molecules are formed by repeatedly applying a sequence of pump—dump pulses. The optimal spectral width of the pump pulse, for photoassociation using a one-photon transition, is obtained from a compromise between our desire to photoassociate at the largest possible internuclear separations and the need to avoid excitation of single atoms, resulting in bandwidths of a few inverse

centimeters. This corresponds to transform-limited pulses of a few picoseconds. The large bandwidth of femtosecond pulses can be utilized only in photoassociation employing multiphoton transitions and pulse shaping to avoid the atomic excitation and subsequent depletion of the ultracold gas. The vibrational structure of the electronically excited state determines the bound−bound Franck−Condon factors and is crucial for successful stabilization, except for very strong field optimal control. Population transfer to bound levels in the ground state is favored if the spin−orbit interaction in the electronically excited state is strong. If absent, an additional laser field can be employed to mimic resonant spin−orbit coupling and engineer the bound−bound Franck−Condon factors.

The number of molecules that can be made by pump−dump photoassociation is limited by the amount of ground state density of atom pairs with sufficiently short interatomic separations. In order to increase the photoassociation rate, control schemes therefore must address the initial thermal cloud of atoms. Both an adiabatic modification of the initial thermal ensemble, employing the control of a scattering resonance, and a nonadiabatic scheme of accelerating atoms toward each other using chirped nanosecond laser pulses, have been studied in order to control the continuum.

Both adiabatic passage and nonadiabatic pump−dump photoassociation need to be combined with a dissipative step in order to repeat the cycle and allow for accumulation of molecules. In the STIRAP scheme we envision that, once formed, molecules are no longer trapped by the laser fields used to trap the atoms. They then fall out of the trap to a secondary trap designed for the molecules where some dissipative process, e.g., evaporation, guarantees trapping. Spatially separated traps could also be employed to avoid dissociation of the formed molecules by the following pair of pump−dump pulses. The rate would then be limited by the time it takes the molecules to leave the atomic trap. Alternatively, a dissipation mechanism that couples directly to the vibrations or rotations of the molecules, e.g., spontaneous emission, could be employed. The decay rate can then be enhanced by a lossy cavity to allow for a high repetition cycle.

Photoassociation based on adiabatic passage and creation of a dark state is best suited to ultracold samples at, or very close to, the quantum degenerate gas limit. In contrast, repeated pump−dump sequences are expected to work best at MOT temperatures, i.e., $T = 1\ \mu\text{K}$ to $T = 100\ \mu\text{K}$. In both cases, the photoassociation reaction differs significantly from that at high temperatures[134] due to the reactants being precorrelated.

AUTHOR INFORMATION

Corresponding Author

*E-mail: christiane.koch@uni-kassel.de; mshapiro@chem.ubc.ca.

Notes

The authors declare no competing financial interest.

Biographies

Christiane Koch studied physics at the Humboldt Universität Berlin and the University of Texas at Austin. She received her Ph.D. degree in Theoretical Physics from the Humboldt Universität Berlin in 2002 after carrying out her thesis work at the Fritz-Haber-Institut der Max-Planck-Gesellschaft under the supervision of Hans-Joachim Freund. She has started to investigate the coherent control of ultracold photoassociation during her postdoctoral studies with Françoise Masnou-Seeuws at Laboratoire Aimé Cotton in Orsay and with Ronnie Kosloff at the Hebrew University Jerusalem. From 2006 to 2010, she headed an independent Emmy Noether junior research group at the Freie Universität Berlin. Since 2010, she is a university professor for Theoretical Physics at the Universität Kassel, where she continues to investigate the coherent control of photoassociation and, more generally, binary reactions at temperatures ranging from ultracold to hot. Her research is dedicated to highlighting the manifestation of quantum mechanical effects in time-dependent phenomena. Besides ultracold molecules, her interests include also the control of open quantum systems and optimal control theory.

Moshe Shapiro holds a B.Sc. in Biochemistry, an M.Sc. in Physical Chemistry, and a Ph.D. in Theoretical Chemistry from the Hebrew University Jerusalem. After a postdoctoral stay at Harvard University in 1970−1972, he joined the Department of Chemical Physics of the Weizmann Institute of Science (WIS) in 1972, where he became a Full Professor in 1983. He served as the department chairman and elected vice chairman of the scientific council of WIS. Shapiro has been a visiting professor at Oxford, Berkeley, several German universities, Arhus, and IMS Okazaki, and he has received numerous prizes. He is an elected fellow of The Institute of Physics and The American Physical Society. Shapiro is the author of more than 300 refereed publications and two textbooks. He holds the Canada Research Chair

S

dx.doi.org/10.1021/cr2003882 | *Chem. Rev.* XXXX, XXX, XXX−XXX

in Quantum Control and is the head of UBC's Peter Wall Institute for Advanced Studies Center for Ultracold Coherent Chemistry.

REFERENCES

(1) Chu, S.; Bjorkholm, J. E.; Ashkin, A.; Cable, A. *Phys. Rev. Lett.* **1986**, *57*, 314.

(2) Aspect, A.; Cohen-Tannoudji, C.; Dalibard, J.; Heidemann, A.; Solomon, C. *Phys. Rev. Lett.* **1986**, *57*, 1688.

(3) Chu, S.; Wieman, C. *J. Opt. Soc. Am. B* **1989**, *6* (11), 2020.

(4) Lawall, J.; Bardou, F.; Shimizu, K.; Leduc, M.; Aspect, A.; Cohen-Tannoudji, C. *Phys. Rev. Lett.* **1994**, *73*, 1915.

(5) Phillips, W. D. *Rev. Mod. Phys.* **1998**, *70*, 721.

(6) Bartana, A.; Kosloff, R.; Tannor, D. J. *J. Chem. Phys.* **1993**, *99*, 196.

(7) Bahns, J. T.; Stwalley, W. C.; Gould, P. L. *J. Chem. Phys.* **1996**, *104*, 9689.

(8) Bartana, A.; Kosloff, R.; Tannor, D. J. *J. Chem. Phys.* **1997**, *106*, 1435.

(9) Bartana, A.; Kosloff, R.; Tannor, D. J. *Chem. Phys.* **2001**, *267*, 195.

(10) Viteau, M.; Chotia, A.; Allegrini, M.; Bouloufa, N.; Dulieu, O.; Comparat, D.; Pillet, P. *Science* **2008**, *321*, 232.

(11) Sofikitis, D.; Fioretti, A.; Weber, S.; Horchania, R.; Pichler, M.; Lia, X.; Allegrini, M.; Chatel, B.; Comparat, D.; Pillet, P. *Mol. Phys.* **2010**, *108*, 795.

(12) Shuman, E. S.; Barry, J. F.; Glenn, D. R.; DeMille, D. *Phys. Rev. Lett.* **2009**, *103*, 223001.

(13) Zeppenfeld, M.; Motsch, M.; Pinkse, P. W. H.; Rempe, G. *Phys. Rev. A* **2009**, *80*, 041401.

(14) Thorsheim, H. R.; Weiner, J.; Julienne, P. S. *Phys. Rev. Lett.* **1987**, *58*, 2420.

(15) Band, Y. B.; Julienne, P. S. *Phys. Rev. A* **1995**, *51*, R4317.

(16) Jones, K. M.; Tiesinga, E.; Lett, P. D.; Julienne, P. S. *Rev. Mod. Phys.* **2006**, *78*, 483.

(17) Fioretti, A.; Comparat, D.; Crubellier, A.; Dulieu, O.; Masnou-Seeuws, F.; Pillet, P. *Phys. Rev. Lett.* **1998**, *80*, 4402.

(18) Gabbanini, C.; Fioretti, A.; Lucchesini, A.; Gozzini, S.; Mazzoni, M. *Phys. Rev. Lett.* **2000**, *84*, 2814.

(19) Dion, C. M.; Drag, C.; Dulieu, O.; Laburthe Tolra, B.; Masnou-Seeuws, F.; Pillet, P. *Phys. Rev. Lett.* **2001**, *86*, 2253.

(20) Kemmann, M.; Mistrik, I.; Nussmann, S.; Helm, H.; Williams, C. J.; Julienne, P. S. *Phys. Rev. A* **2004**, *69*, 022715.

(21) Masnou-Seeuws, F.; Pillet, P. *Adv. At., Mol., Opt. Phys.* **2001**, *47*, 53.

(22) Vardi, A.; Abrashkevich, D.; Frishman, E.; Shapiro, M. *J. Chem. Phys.* **1997**, *107*, 6166.

(23) Côté, R.; Dalgarno, A. *Chem. Phys. Lett.* **1997**, *279*, 50.

(24) Julienne, P. S.; Burnett, K.; Band, Y. B.; Stwalley, W. C. *Phys. Rev. A* **1998**, *58*, R797.

(25) Vardi, A.; Shapiro, M.; Bergmann, K. *Opt. Express* **1999**, *4*, 91.

(26) Mackie, M.; Javanainen, J. *Phys. Rev. A* **1999**, *60*, 3174.

(27) Vardi, A.; Shapiro, M. *Phys. Rev. A* **2000**, *62*, 025401.

(28) Mackie, M.; Kowalski, R.; Javanainen, J. *Phys. Rev. Lett.* **2000**, *84*, 3803.

(29) Vardi, A.; Shapiro, M. *Phys. Rev. A* **1998**, *58*, 1352.

(30) Vardi, A.; Shapiro, M.; Anglin, J. R. *Phys. Rev. A* **2002**, *65*, 027401.

(31) Drummond, P. D.; Kheruntsyan, K. V.; Heinzen, D. J.; Wynar, R. H. *Phys. Rev. A* **2002**, *65*, 063619.

(32) Ling, H.; Pu, H.; Seaman, B. *Phys. Rev. Lett.* **2004**, *93*, 250403.

(33) Kuznetsova, E.; Pellegrini, P.; Côté, R.; Lukin, M. D.; Yelin, S. F. *Phys. Rev. A* **2008**, *78*, 021402.

(34) Kuznetsova, E.; Gacesa, M.; Pellegrini, P.; Yelin, S. F.; Côté, R. *New J. Phys.* **2009**, *11*, 055028.

(35) Vala, J.; Dulieu, O.; Masnou-Seeuws, F.; Pillet, P.; Kosloff, R. *Phys. Rev. A* **2001**, *63*, 013412.

(36) Luc-Koenig, E.; Kosloff, R.; Masnou-Seeuws, F.; Vatasescu, M. *Phys. Rev. A* **2004**, *70*, 033414.

(37) Luc-Koenig, E.; Masnou-Seeuws, F.; Vatasescu, M. *Eur. Phys. J. D* **2004**, *31*, 239.

(38) Koch, C. P.; Luc-Koenig, E.; Masnou-Seeuws, F. *Phys. Rev. A* **2006**, *73*, 033408.

(39) Koch, C. P.; Kosloff, R.; Masnou-Seeuws, F. *Phys. Rev. A* **2006**, *73*, 043409.

(40) Koch, C. P.; Moszyński, R. *Phys. Rev. A* **2008**, *78*, 043417.

(41) Koch, C. P. *Phys. Rev. A* **2008**, *78*, 063411.

(42) Hulet, R. G. Coherence in Photoassociation of a Quantum Degenerate Gas. In *Cold Molecules and Bose-Einstein Condensates*; Les Houches, France, 2002.

(43) Dumke, R.; Weinstein, J. D.; Johanning, M.; Jones, K. M.; Lett, P. D. *Phys. Rev. A* **2005**, *72*, 041801.

(44) Winkler, K.; Thalhammer, G.; Theis, M.; Ritsch, H.; Grimm, R.; Denschlag, J. H. *Phys. Rev. Lett.* **2005**, *95*, 063202.

(45) Ni, K.-K.; Ospelkaus, S.; de Miranda, M. H. G.; Pe'er, A.; Neyenhuis, B.; Zirbel, J. J.; Kotochigova, S.; Julienne, P. S.; Jin, D. S.; Ye, J. *Science* **2008**, *322*, 231.

(46) Regal, C. A.; Ticknor, C.; Bohn, J. L.; Jin, D. S. *Nature* **2003**, *424*, 47.

(47) Strecker, K. E.; Partridge, G. B.; Hulet, R. G. *Phys. Rev. Lett.* **2003**, *91*, 080406.

(48) Winkler, K.; Lang, F.; Thalhammer, G.; v. d. Straten, P.; Grimm, R.; Denschlag, J. H. *Phys. Rev. Lett.* **2007**, *98*, 043201.

(49) Ospelkaus, S.; Pe'er, A.; Ni, K.-K.; Zirbel, J. J.; Neyenhuis, B.; Kotochigova, S.; Julienne, P. S.; Ye, J.; Jin, D. S. *Nature Phys.* **2008**, *4*, 622.

(50) Lang, F.; Winkler, K.; Strauss, C.; Grimm, R.; Denschlag, J. H. *Phys. Rev. Lett.* **2008**, *101*, 133005.

(51) Danzl, J. G.; Haller, E.; Gustavsson, M.; Mark, M. J.; Hart, R.; Bouloufa, N.; Dulieu, O.; Ritsch, H.; Nägerl, H.-C. *Science* **2008**, *321*, 1062.

(52) Spiegelhalder, F.; Trenkwalder, A.; Naik, D.; Kerner, G.; Wille, E.; Hendl, G.; Schreck, F.; Grimm, R. *Phys. Rev. A* **2010**, *81*, 043637.

(53) Bergmann, K.; Theuer, H.; Shore, B. W. *Rev. Mod. Phys.* **1998**, *70*, 1003.

(54) Shapiro, M. *J. Chem. Phys.* **1994**, *101*, 3849.

(55) Vardi, A.; Shapiro, M. *J. Chem. Phys.* **1996**, *104*, 5490.

(56) Marvet, U.; Dantus, M. *Chem. Phys. Lett.* **1995**, *245*, 393.

(57) Gross, P.; Dantus, M. *J. Chem. Phys.* **1997**, *106*, 8013.

(58) Nikolov, A. N.; Eyler, E. E.; Wang, X. T.; Li, J.; Wang, H.; Stwalley, W.; Gould, P. L. *Phys. Rev. Lett.* **1999**, *82*, 703.

(59) Wynar, R.; Freeland, R.; Han, D.; Ryu, C.; Heinzen, D. *Science* **2000**, *287*, 1016.

(60) McKenzie, C.; et al. *Phys. Rev. Lett.* **2002**, *88*, 120403.

(61) Shapiro, E. A.; Shapiro, M.; Pe'er, A.; Ye, J. *Phys. Rev. A* **2007**, *75*, 013405.

(62) Spiegelmann, F.; Pavolini, D.; Daudey, J.-P. *J. Phys. B: At. Mol. Opt. Phys.* **1989**, *22*, 2465.

(63) Edvardsson, D.; Lunell, S.; Marian, C. M. *Mol. Phys.* **2003**, *101*, 2381.

(64) Marinescu, M.; Sadeghpour, H. R.; Dalgarno, A. *Phys. Rev. A* **1994**, *49*, 982.

(65) Landau, L. D.; Lifshitz, E. M. *Quantum mechanics: Non-relativistic theory*; Butterworth-Heinemann: Oxford, 1981.

(66) Weiner, J.; Bagnato, V. S.; Zilio, S.; Julienne, P. S. *Rev. Mod. Phys.* **1998**, *71*, 1.

(67) Roberts, J. L.; Claussen, N.; Burke, J. P., Jr.; Greene, C. H.; Cornell, E. A.; Wieman, C. E. *Phys. Rev. Lett.* **1998**, *81*, 5109.

(68) Vogels, J. M.; Tsai, C. C.; Freeland, R. S.; Kokkelmans, S. J. J. M. F.; Verhaar, B. J.; Heinzen, D. J. *Phys. Rev. A* **1997**, *56*, R1067.

(69) Vitanov, N. V.; Stenholm, S. *Phys. Rev. A* **1999**, *60*, 3820.

(70) Pe'er, A.; Shapiro, E. A.; Stowe, M. C.; Shapiro, M.; Ye, J. *Phys. Rev. Lett.* **2007**, *98*, 113004.

(71) Coulston, G.; Bergmann, K. *J. Chem. Phys.* **1992**, *96*, 3467.

(72) Theuer, H.; Unanyan, R. G.; Habschied, C.; Klein, K.; Bergmann, K. *Opt. Express* **1999**, *4*, 77.

(73) Kobrak, M. N.; Rice, S. A. *Phys. Rev. A* **1998**, *57*, 2885.

(74) Král, P.; Shapiro, M. *Phys. Rev. A* **2002**, *65*, 043413.

(75) Lang, F.; Strauss, C.; Winkler, K.; Takekoshi, T.; Grimm, R.; Denschlag, J. H. *Faraday Discuss.* **2009**, *142*, 271.

(76) Pilch, K.; Lange, A. D.; Prantner, A.; Kerner, G.; Ferlaino, F.; Nägerl, H.-C.; Grimm, R. *Phys. Rev. A* **2009**, *79*, 042718.

(77) Köhler, T.; Góral, K.; Julienne, P. S. *Rev. Mod. Phys.* **2006**, *78*, 1311.

(78) Ospelkaus, C.; Ospelkaus, S.; Humbert, L.; Ernst, P.; Sengstock, K.; Bongs, K. *Phys. Rev. Lett.* **2006**, *97*, 120402.

(79) Zirbel, J. J.; Ni, K.-K.; Ospelkaus, S.; Incao, J. P. D.; Wieman, C. E.; Ye, J.; Jin, D. S. *Phys. Rev. Lett.* **2008**, *100*, 143201.

(80) Zirbel, J. J.; Ni, K.-K.; Ospelkaus, S.; Nicholson, T. L.; Olsen, M. L.; Julienne, P. S.; Wieman, C. E.; Ye, J.; Jin, D. S. *Phys. Rev. A* **2008**, *78*, 013416.

(81) Markiewisz, M.; Kraemer, T.; Waldburger, P.; Herbig, J.; Chin, C.; Nägerl, H.-C.; Grimm, R. *Phys. Rev. Lett.* **2007**, *99*, 113201.

(82) Knoop, S.; Ferlaino, F.; Mark, M.; Berninger, M.; Schöbel, H.; Nägerl, H.-C.; Grimm, R. *Nat. Phys.* **2009**, *5*, 227.

(83) Knoop, S.; Ferlaino, F.; Berninger, M.; Mark, M.; Nägerl, H.-C.; Grimm, R.; D'Incao, J. P.; Esry, B. *Phys. Rev. Lett.* **2010**, *104*, 053201.

(84) Ospelkaus, S.; Ni, K.-K.; Wang, D.; de Miranda, M. H. G.; Neyenhuis, B.; Quéméner, G.; Julienne, P. S.; Bohn, J. L.; Jin, D. S.; Ye, J. *Science* **2010**, *327*, 853.

(85) Fatemi, F.; Jones, K. M.; Wang, H.; Walmsley, I.; Lett, P. D. *Phys. Rev. A* **2001**, *64*, 033421.

(86) In the quantum degenerate gas regime, a purely coherent molecule formation scheme addressing the whole ensemble in a single step is preferrable. This has been realized, for example, by Feshbach association in combination with STIRAP as discussed above.

(87) Crubellier, A.; Luc-Koenig, E. *J. Phys. B* **2006**, *39*, 1417.

(88) Koch, C. P.; Kosloff, R.; Luc-Koenig, E.; Masnou-Seeuws, F.; Crubellier, A. *J. Phys. B* **2006**, *39*, S1017.

(89) Kallush, S.; Kosloff, R.; Masnou-Seeuws, F. *Phys. Rev. A* **2007**, *75*, 043404.

(90) $\varphi_{nJ}(R)$ is an eigenfunction of the computation box, normalized to unity. "True" energy-normalized scattering wave functions are straightforwardly obtained from $\varphi_{nJ}(R)$, provided the box eigenvalues are sufficiently closely spaced to approximate the continuum of scattering energies.[37,88,89]

(91) Salzmann, W.; Poschinger, U.; Wester, R.; Weidemüller, M.; Merli, A.; Weber, S. M.; Sauer, F.; Plewicki, M.; Weise, F.; Mirabal Esparza, A.; Wöste, L.; Lindinger, A. *Phys. Rev. A* **2006**, *73*, 023414.

(92) Brown, B. L.; Dicks, A. J.; Walmsley, I. A. *Phys. Rev. Lett.* **2006**, *96*, 173002.

(93) Koch, C. P.; Ndong, M.; Kosloff, R. *Faraday Discuss.* **2009**, *142*, 389.

(94) Meshulach, D.; Silberberg, Y. *Nature* **1998**, *396*, 239.

(95) Meshulach, D.; Silberberg, Y. *Phys. Rev. A* **1999**, *60*, 1287.

(96) Trallero-Herrero, C.; Cardoza, D.; Weinacht, T. C.; Cohen, J. L. *Phys. Rev. A* **2005**, *71*, 013423.

(97) Trallero-Herrero, C.; Cohen, J. L.; Weinacht, T. *Phys. Rev. Lett.* **2006**, *96*, 063603.

(98) Koch, C. P.; Palao, J. P.; Kosloff, R.; Masnou-Seeuws, F. *Phys. Rev. A* **2004**, *70*, 013402.

(99) Note that chirping the pulse may be used to enforce adiabatic following conditions and thus complete population transfer *within* the photoassociation window.[36,37]

(100) Zeman, V.; Shapiro, M.; Brumer, P. *Phys. Rev. Lett.* **2004**, *92*, 133204.

(101) Pellegrini, P.; Gacesa, M.; Côté, R. *Phys. Rev. Lett.* **2008**, *101*, 053201.

(102) Han, A.; Shapiro, E.; Shapiro, M. *J. Phys. B* **2011**, *44*, 154018.

(103) Krems, R. V. *Phys. Rev. Lett.* **2006**, *96*, 123202.

(104) González-Férez, R.; Schmelcher, P. *New J. Phys.* **2009**, *11*, 055013.

(105) Chakraborty, D.; Hazra, J.; Deb, B. *J. Phys. B* **2011**, *44*, 095201.

(106) Boesten, H. M. J. M.; Tsai, C. C.; Verhaar, B. J.; Heinzen, D. J. *Phys. Rev. Lett.* **1996**, *77*, 5194.

(107) Boesten, H. M. J. M.; Tsai, C. C.; Gardner, J. R.; Heinzen, D. J.; Verhaar, B. J. *Phys. Rev. A* **1997**, *55*, 636.

(108) Londoño, B. E.; Mahecha, J. E.; Luc-Koenig, E.; Crubellier, A. *Phys. Rev. A* **2010**, *82*, 012510.

(109) Ağanoğlu, R.; Lemeshko, M.; Friedrich, B.; González-Férez, R.; Koch, C. P. *arXiv:*1105.0761, 2011.

(110) Wright, M. J.; Gensemer, S. D.; Vala, J.; Kosloff, R.; Gould, P. L. *Phys. Rev. Lett.* **2005**, *95*, 063001.

(111) Wright, M. J.; Pechkis, J. A.; Carini, J. L.; Gould, P. L. *Phys. Rev. A* **2006**, *74*, 063402.

(112) Kallush, S.; Kosloff, R. *Phys. Rev. A* **2007**, *76*, 053408.

(113) Luc-Koenig, E.; Masnou-Seeuws, F. m. c.; Kosloff, R. *Phys. Rev. A* **2007**, *76*, 053415.

(114) Kallush, S.; Kosloff, R. *Phys. Rev. A* **2008**, *77*, 023421.

(115) Pechkis, H. K.; Wang, D.; Huang, Y.; Eyler, E. E.; Gould, P. L.; Stwalley, W. C.; Koch, C. P. *Phys. Rev. A* **2007**, *76*, 022504.

(116) Fioretti, A.; Dulieu, O.; Gabbanini, C. *J. Phys. B* **2007**, *40*, 3283.

(117) Ghosal, S.; Doyle, R. J.; Koch, C. P.; Hutson, J. M. *New J. Phys.* **2009**, *11*, 055011.

(118) Tomza, M.; Pawłowski, F.; Jeziorska, M.; Koch, C. P.; Moszynski, R. *Phys. Chem. Chem. Phys.* **2011**, *13*, 18893.

(119) Ulmanis, J.; Deiglmayr, J.; Wester, R.; Weidemüller, M. *Chem. Rev.* In preparation.

(120) Salzmann, W.; Mullins, T.; Eng, J.; Albert, M.; Wester, R.; Weidemüller, M.; Merli, A.; Weber, S. M.; Sauer, F.; Plewicki, M.; Weise, F.; Wöste, L.; Lindinger, A. *Phys. Rev. Lett.* **2008**, *100*, 233003.

(121) Mullins, T.; Salzmann, W.; Götz, S.; Albert, M.; Eng, J.; Wester, R.; Weidemüller, M.; Weise, F.; Merli, A.; Weber, S. M.; Sauer, F.; Wöste, L.; Lindinger, A. *Phys. Rev. A* **2009**, *80*, 063416.

(122) McCabe, D. J.; England, D. G.; Martay, H. E. L.; Friedman, M. E.; Petrovic, J.; Dimova, E.; Chatel, B.; Walmsley, I. A. *Phys. Rev. A* **2009**, *80*, 033404.

(123) Merli, A.; Eimer, F.; Weise, F.; Lindinger, A.; Salzmann, W.; Mullins, T.; Götz, S.; Wester, R.; Weidemüller, M.; Ağanoğlu, R.; Koch, C. P. *Phys. Rev. A* **2009**, *80*, 063417.

(124) Weise, F.; Merli, A.; Eimer, F.; Birkner, S.; Sauer, F.; Wöste, L.; Lindinger, A.; Salzmann, W.; Mullins, T.; Götz, S.; Wester, R.; Weidemüller, M.; Ağanoğlu, R.; Koch, C. P. *J. Phys. B* **2009**, *42*, 215307.

(125) Eimer, F.; Weise, F.; Merli, A.; Birkner, S.; Sauer, F.; Wöste, L.; Lindinger, A.; Ağanoğlu, R.; Koch, C. P.; Salzmann, W.; Mullins, T.; Götz, S.; Wester, R.; Weidemüller, M. *Eur. Phys. J. D* **2009**, *54*, 711.

(126) Sofikitis, D.; Weber, S.; Fioretti, A.; Horchani, R.; Allegrini, M.; Chatel, B.; Comparat, D.; Pillet, P. *New J. Phys.* **2009**, *11*, 055037.

(127) Sofikitis, D.; Horchani, R.; Li, X.; Pichler, M.; Allegrini, M.; Fioretti, A.; Comparat, D.; Pillet, P. *Phys. Rev. A* **2009**, *80*, 051401.

(128) Viteau, M.; Chotia, A.; Allegrini, M.; Bouloufa, N.; Dulieu, O.; Comparat, D.; Pillet, P. *Phys. Rev. A* **2009**, *79*, 021402.

(129) Viteau, M.; Chotia, A.; Sofikitis, D.; Allegrini, M.; Bouloufa, N.; Dulieu, O.; Comparat, D.; Pillet, P. *Faraday Discuss.* **2009**, *142*, 257.

(130) Koch, C. P.; Kosloff, R. *Phys. Rev. Lett.* **2009**, *103*, 260401.

(131) Koch, C. P.; Kosloff, R. *Phys. Rev. A* **2010**, *81*, 063426.

(132) Köhler, T.; Burnett, K. *Phys. Rev. A* **2002**, *65*, 033601.

(133) Naidon, P.; Masnou-Seeuws, F. *Phys. Rev. A* **2003**, *68*, 033612.

(134) Rybak, L.; Amaran, S.; Levin, L.; Tomza, M.; Moszynski, R.; Kosloff, R.; Koch, C. P.; Amitay, Z. *Phys. Rev. Lett.* **2011**, *107*, 273001.